Check for updates

MICROBIOLOGY

Establishment of titration-based control of DNA replication in *Escherichia coli*

Belén Adiego-Pérez[1], Christina Ludwig[2], Demian Fluit[3], Mareike Berger[4], Alejandra Alonso Santirso[1], Johannes Hohlbein[3,5]†, Raymond H. J. Staals[1], Pieter Rein ten Wolde[4], John van der Oost[1], Nico J. Claassens[1], Lorenzo Olivi[1]‡*

Copyright © 2026 The Authors, some rights reserved; exclusive licensee American Association for the Advancement of Science. No claim to original U.S. Government Works. Distributed under a Creative Commons Attribution License 4.0 (CC BY).

Escherichia coli **couples the initiation of DNA replication with cell size by modulating the activity of the replication initiator protein DnaA. The activity of DnaA is regulated both by its interconversion between an active and inactive form and by its titration on chromosomal binding sites. Whereas its interconversion has been thoroughly studied, the extent to which DnaA titration can control replication initiation is poorly understood. Here, we describe the control of *E. coli* DNA replication via titration by modulating the expression of a constitutively active DnaA variant in four growth conditions. While we obtained stable cell cycles during slow growth, faster growth associated with overlapping replication forks led to initiation instability and replicative stress. Overall, our results provide insights into the limits of titration-based systems in the control of genome replication and their potential role in the evolutionary trajectory of *E. coli*. Last, this study provides design principles for a simplified, titration-only regulatory mechanism for DNA replication in synthetic cells.**

INTRODUCTION

Precise control over genome replication is crucial for optimal fitness of all forms of life. In most studied bacteria, the initiation of DNA replication relies on the replication initiator protein DnaA (*1*). The binding of DnaA to specific DNA motifs (DnaA boxes) present at the origin of replication of the bacterial chromosome causes local melting of the double-stranded DNA structure and recruitment of the proteins of the replisome complex (*2*, *3*). Uncontrolled initiation of DNA replication is associated with hyper-replicative stress and generally leads to severe fitness loss (*4*, *5*). Thus, several mechanisms are in place to ensure that DnaA binds and unwinds the origin only when specific conditions are met.

In *Escherichia coli*, cells coordinate DNA replication with growth (*6*, *7*), such that initiation occurs at a constant cellular volume per number of origins (*7*, *8*). At fast growth, this coupling results in the presence of multiple replication forks in a single chromosome, which allows cells to divide faster than the time needed to replicate their chromosome (*9*, *10*). The known mechanisms controlling this characteristic behavior are the regulation of both production and activity of the DnaA protein. First, the near-balanced expression of the *dnaA* gene results in constant intracellular DnaA concentrations (*11*), with the specific concentration value set by the growth rate (*12*). Second, DnaA exists either in an active or an inactive form, bound to adenosine triphosphate (ATP) or adenosine diphosphate (ADP), respectively (*13*). De novo synthesized DnaA predominantly binds to ATP, due to its higher abundance in the cell compared to ADP (*14*). The ratio of the two forms is then controlled by several mechanisms. Interaction with either noncoding loci *DARS1* and *DARS2* (*15*) or acid phospholipids at the cell membrane (*16*) promotes the exchange of the nucleotide bound to DnaA from ADP to ATP, reactivating the protein. On the other hand, DnaA is also recruited on the noncoding sequence *datA*, where the protein is inactivated via *datA*-mediated DnaA-ATP hydrolysis (*17*). Last, DnaA is also inactivated by the action of the protein Hda, which associates with the β-clamp of DNA polymerase III during replication to stimulate hydrolysis of DnaA-bound ATP (*18*). Only the active, ATP-bound form can unwind the origin of replication (*oriC*) (*19*–*21*). Thus, accumulation of DnaA-ATP to a certain threshold value is a critical step in the initiation of DNA replication (*22*). At the same time, the titration of DnaA on DNA boxes spread across the chromosome of *E. coli* also acts in regulating replication initiation (*23*, *24*). In this titration model, the free concentration of DnaA is maintained at a low level through sequestration of the protein on high-affinity DnaA boxes spread across the chromosome. Once these titration sites are saturated, the free concentration of DnaA rises until low affinity DnaA boxes present on *oriC* become occupied (*19*), eventually resulting in initiation of replication. Although evidence on the effect of titration has historically been scarce, recent studies support a scenario where a combination of both mechanisms orchestrates cell cycles in *E. coli*. Previously, we probed the mobility of DnaA in live *E. coli* cells and demonstrated that its titration plays a role in the control of DNA replication during slow growth (*25*). Cell cycle simulations also predicted that only the combination of titration and interconversion of DnaA yields stable replication cycles across growth conditions (*26*, *27*). Last, additional indirect evidence comes from the fact that reaching peak levels of DnaA-ATP is necessary but not sufficient to initiate DNA replication (*28*), hinting at DnaA titration being responsible for the observed delay.

To date, the extent to which DnaA titration alone can contribute to the regulation of DNA replication is still unclear. Here, we used a homeostatic, inducible genetic circuit to control the expression of the mutant DnaA cold-sensitive allele (DnaAcos), a variant impaired in nucleotide binding (*29*). This modification abolishes interconversion

[1]Laboratory of Microbiology, Wageningen University & Research, Wageningen, Netherlands. [2]Bavarian Center for Biomolecular Mass Spectrometry (BayBioMS), School of Life Sciences, Technical University of Munich, Munich, Germany. [3]Laboratory of Biophysics, Wageningen University & Research, Wageningen, Netherlands. [4]Institute AMOLF, Amsterdam, Netherlands. [5]Microspectroscopy Research Facility, Wageningen University & Research, Wageningen, Netherlands.
*Corresponding author. Email: lorenzo.olivi@icm.uu.se
†Present address: FG Biosensorics, Institute of Biotechnology, Faculty of Environment and Natural Sciences, Brandenburg University of Technology Cottbus-Senftenberg, Senftenberg, Germany.
‡Present address: Department of Cell and Molecular Biology, Science for Life Laboratory, Uppsala University, Uppsala, Sweden.

Downloaded from https://www.science.org at AMOLF on November 11, 2026

between active and inactive DnaA and leaves titration as the only remaining, known control mechanism for DNA replication. This genetic system allowed us to experimentally confirm predictions of DNA replication instability in *E. coli* in the absence of an ATP/ADP switch in regimes of overlapping replication forks (*26*), which should lead to an unviable phenotype (*4*). Unexpectedly, the selection of a missense mutation in the DnaB helicase gene restored growth in all the tested conditions. We thus analyzed the phenotype of the resulting *E. coli* coregulatory TetR-DnaAcos (*E. coli* CoRTeDcos) strain in different growth conditions and induction levels by measuring a variety of cellular parameters in parallel. We conclude that a titration-based system recreates the phenomenon of constant volumes of initiation across growth conditions and that this volume is uniquely set by the concentration of DnaAcos. Nevertheless, proteomic analysis revealed signs of hyper-replicative stress in *E. coli* CoRTeDcos under conditions that promote overlapping replication forks. Together, our results bring new perspectives on DnaA titration as a form of control of DNA replication initiation and provide valuable insights for the eventual design of controlled genetic inheritance systems in synthetic cells.

RESULTS

Construction of an *E. coli* strain incapable of DnaA-ATP/DnaA-ADP switch

In this study, we sought to create a molecular mechanism based on titration that recreates the phenomenological observation of a constant initiation volume across growth rates. To achieve this behavior, several design criteria needed to be met. First, the native switch between DnaA-ATP and DnaA-ADP had to be abolished. An *E. coli* strain with deletions for of all known loci involved in the interconversion between the two forms has already been reported (*11*). Yet, this strain was still capable of cycling between the two forms via the intrinsic adenosine triphosphatase activity of DnaA and the binding of ATP upon de novo synthesis (*11*). Thus, we decided to replace the wild-type DnaA with the mutant allele DnaAcos. DnaAcos was originally obtained as an intragenic suppressor of the temperature-sensitive variant DnaA46 (*30*, *31*), with which it shares two amino acid substitutions that impair nucleotide binding (A184V and H252Y) (*29*, *32*). In DnaAcos, two additional substitutions (Q156L and Y271H) stabilize the protein activity below 42°C (*29*, *33*). As a consequence, DnaAcos is constitutively active in initiating DNA replication in the normal range of *E. coli* culturing temperatures (*29*). Next, in pure titration-based systems, the rate at which DnaA is synthesized dictates both the mass fraction of DnaA (ϕ_{DnaA}) and how quickly the DnaA boxes on the chromosome are saturated. Since the saturation of DnaA boxes leads to *oriC* binding and initiation of DNA replication, higher ϕ_{DnaA} then result in smaller volumes at initiation (*26*). Thus, achieving constant volumes of initiation across growth rates means implementing an expression system that maintains ϕ_{DnaA} constant independently of nutrient conditions. In wild-type *E. coli* wild-type, ϕ_{DnaA} varies of ~50% across growth rates (*12*). To achieve constant and controllable ϕ_{DnaA} across growth rates, we selected a genetic circuit where the expression of DnaAcos is controlled by a negatively autoregulated TetR repressor (*34*). This type of genetic architecture should provide stable mass fractions of the coregulated protein (i.e., DnaAcos) across growth rates, with the added benefit of controlling such concentration via addition of the inducer molecule anhydrotetracycline (aTc) (*34*). Last, replication needs to be initiated when a critical threshold of DnaAcos proteins has accumulated. In DnaA titration-based system, this threshold is set by the number of high-affinity DnaA boxes that need to be saturated before DnaA can bind and unwind *oriC* (*23*, *26*). Previously, we showed that the chromosome of *E. coli* is capable of titrating DnaA (*25*). Hence, we chose to rely on the hundreds of native DnaA boxes distributed across the *E. coli* chromosome to govern the accumulation of DnaA toward its critical threshold.

Following these design principles, we replaced the wild-type *E. coli dnaA* gene and its promoters with a coregulatory construct composed of the $P_{LtetO-1}$ promoter, the *tetR* repressor gene, and the *dnaAcos* gene (Fig. 1A). SeqA-mediated repression of DnaAcos was also abolished by removing GATC motifs on the P_{dnaA} promoter (*35*, *36*). Blockage of *oriC* during the eclipse period was maintained (*35*, *36*). Notably, a coregulatory construct yields low levels of protein production even in the absence of the inducer (*34*), ensuring DNA replication initiation and viability of our strain in the absence of aTc. After successfully obtaining the mutant strain, we first characterized its growth phenotype in two growth media and five concentrations of aTc (Fig. 1B and fig. S1). The obtained strain was viable in poor nutrient medium leading to slow growth in a variety of aTc concentrations, with growth rates slightly lower than the wild type ($\lambda_{WT} = 0.27 \pm 0.015$ hour^{-1}, $\lambda_{mutant} = 0.207 \pm 0.015$ hour^{-1}). However, when cultivated in a medium leading to overlapping replication regime in the wild type ($\lambda_{WT} = 0.987 \pm 0.016$ hour^{-1}), the mutant strain was incapable to grow at concentrations of aTc of 10 ng/ml or higher. Notably, prolonged incubation in the same conditions yielded an evolved strain capable of proliferating at high growth rates and across a large range of aTc concentrations (Fig. 1B).

Initiator titration systems are predicted to be unstable at growth rates leading to overlapping replication regimes (*26*, *27*). These predictions are in line with the known hyper-replicative stress phenotype associated with DnaAcos (*4*, *29*, *33*) and likely explain the lack of viability of the original mutant strain in fast growth conditions. The evolved strain is capable of surviving in the same conditions without any mutations in the coregulatory *tetR-dnaAcos* locus nor any previously reported mutation rescuing hyper-replicative phenotypes (*37*–*40*). Rather, we observed a single mutation in the replicative DNA helicase *dnaB* gene, leading to an M242I amino acid substitution. This mutation is known to cause several defects, resulting in a DNA helicase hexamer with reduced unwinding capacity (*41*). The selection of this mutation restored viability of the strain in a large range of growth conditions. We thus decided to further characterize this strain, which we named *E. coli* CoRTeDcos. We first attempted to obtain the average number of origins in slow-growing ($\lambda \approx 0.3$ hour^{-1}) *E. coli* CoRTeDcos populations via rifampicin and cephalexin-mediated cell cycle synchronization. Notably, we noticed that we could not obtain populations of cells with a defined number of origins within the 6 hours of antibiotic treatment, in contrast to wild-type *E. coli* (fig. S2). This behavior can be explained by high levels of active DnaA that keep firing new replicative events even after *dnaA* transcription is halted by rifampicin (*42*–*44*). In *E. coli* CoRTeDcos, roughly defined populations of cells were observed in the absence of aTc, but this resolution progressively worsened with increasing inducer concentrations (fig. S2). This dose dependence indicates that stronger expression of DnaAcos leads to a longer period of sustained initiations after transcription arrest, in line with the fact that this protein variant is constitutively active (*29*).

Downloaded from https://www.science.org at AMOLF on November 11, 2026

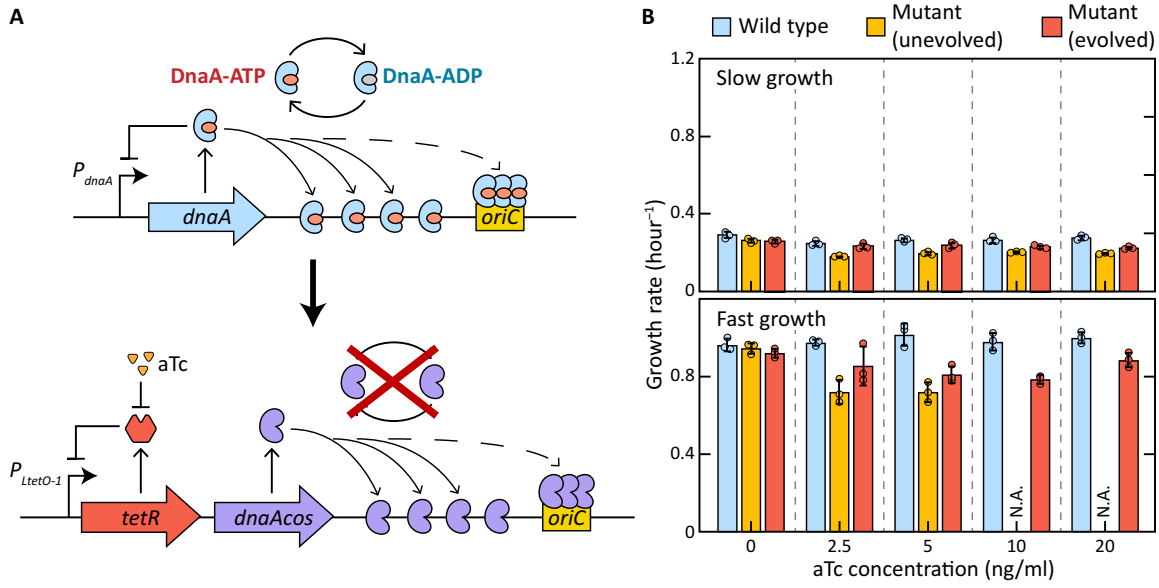


Fig. 1. Design and characterization of *E. coli* CoRTeDcos. (**A**) Design of a genetic architecture allowing for titration-based control of DNA replication in *E. coli*. Top: native *dnaA* locus in *E. coli*. Bottom: engineered locus in *E. coli* CoRTeDcos strain. (**B**) Growth rate of the wild-type *E. coli* MG1655 (blue), the initial mutant strain (yellow), and the final *E. coli* CoRTeDcos strain (red) after the selection of the DnaB(M242I) substitution. Media leading to slow growth (top) or fast growth and overlapping replication forks (bottom) were tested in the presence of varying concentrations of aTc. The final *E. coli* CoRTeDcos strain was selected during fast growth conditions and in the presence of aTc. Growth curves are available in the Supplementary Materials (fig. S1).

Quantitative cell cycle relations in the absence of DnaA-ATP/ADP interconversion

To assess the replicative behavior of *E. coli* CoRTeDcos, we leveraged turbidostat cultivations to balance cells in exponential growth (*7*, *12*, *25*, *45*) and performed population-level measurements of relevant cellular parameters (*7*). We first benchmarked our strategy by reproducing known behaviors of wild-type *E. coli* across different nutrient conditions (fig. S3). We then moved to compare the behavior of the wild-type *E. coli* MG1655 and the mutant *E. coli* CoRTeDcos in four different media supporting growth at different growth rates (M1 to M4; see table S2 for composition) and two levels of aTc (0 and 10 ng/ml) (Fig. 2). In media M1 and M2 ($\lambda_{WT\text{-}M1} = 0.36 \pm 0.03$ hour^{-1}, $\lambda_{WT\text{-}M2} = 0.64 \pm 0.02$ hour^{-1}), *E. coli* CoRTeDcos grew similarly to the wild type at either 0 or 10 ng/ml of aTc ($\lambda_{CoRTeDcos\text{-}M1\text{-}0} = 0.34 \pm 0.03$ hour^{-1}, $\lambda_{CoRTeDcos\text{-}M1\text{-}10} = 0.38 \pm 0.02$ hour^{-1}; $\lambda_{CoRTeDcos\text{-}M2\text{-}0} = 0.65 \pm 0.02$ hour^{-1}, $\lambda_{CoRTeDcos\text{-}M2\text{-}10} = 0.67 \pm 0.02$ hour^{-1}). In more nutrient-rich conditions leading to overlapping replication forks, the presence of the mutant locus led to a reduction of growth rate. In medium M3, *E. coli* CoRTeDcos grew consistently slower than the wild type, with the presence of aTc eliciting no additional effect ($\lambda_{WT} = 1.25 \pm 0.02$ hour^{-1}, $\lambda_{CoRTeDcos\text{-}M3\text{-}0} = 1.04 \pm 0.01$ hour^{-1}, $\lambda_{CoRTeDcos\text{-}M3\text{-}10} = 1.08 \pm 0.03$ hour^{-1}). At even faster growth rates ($\lambda_{WT\text{-}M4} = 1.83 \pm 0.05$ hour^{-1}), the presence of inducer seemed to further affect growth ($\lambda_{CoRTeDcos\text{-}M4\text{-}0} = 1.45 \pm 0.03$ hour^{-1}, $\lambda_{CoRTeDcos\text{-}M4\text{-}10} = 1.28 \pm 0.08$ hour^{-1}). To characterize the expression behavior of the coregulatory construct, we obtained ϕ_{DnaA} via quantitative proteomics (Fig. 2B). In the absence of inducer, the $\phi_{DnaAcos}$ doubled across growth rates while remaining around 5.5 lower than the ϕ_{DnaA} in wild-type cells. In the presence of 10 ng/ml of aTc, the coregulatory construct yielded constant $\phi_{DnaAcos}$, varying by only 0.7% across five-fold increases of growth rate. In contrast, the wild-type ϕ_{DnaA} varied of 43% in the same range of growth rates, similarly to what had previously been shown (*12*).

E. coli CoRTeDcos recapitulates many known general relationships between growth rate and cell cycle even in the absence of DnaA-ATP/DnaA-ADP interconversion. Both cellular volume (Fig. 2C) and number of origins (Fig. 2D) scaled exponentially with growth rate, in agreement with the general growth law (*7*, *12*, *46*). At the same time, the volume of initiation remained roughly constant (Fig. 2E). The increase in $\phi_{DnaAcos}$ due to the presence of aTc had a clear effect on all these parameters. Specifically, larger $\phi_{DnaAcos}$ led to a decrease in volume and an increase in the number of origins. Even in this new condition, both parameters still increased exponentially with growth rate. The volume of initiation of *E. coli* CoRTeDcos cultured in 10 ng/ml of aTc was lower than the one obtained in the absence of aTc and remained roughly constant across growth rates. The observed effect of an increase in $\phi_{DnaAcos}$ is consistent with the predicted behavior of a previously described model of titration-based control of DNA replication (*26*). In this type of systems, the initiation size is set by the accumulation of enough DnaA to saturate the high-affinity motifs present on the chromosome (*26*, *47*). Thus, increased synthesis of DnaAcos leads to faster occupation of these titration sites and earlier initiation events, reducing the average volume and increasing the number of origins of the population.

E. coli CoRTeDcos replication initiation behaves as a titration-based system

After observing growth-related phenotypes, we decided to further investigate the response of *E. coli* CoRTeDcos at varying aTc concentrations. We selected media M1, leading to slow growth, and M3, which yields a condition of fast growth with overlapping replication forks. We then used a total of eight different aTc concentrations to vary the $\phi_{DnaAcos}$ and probe its effect on the strain physiology.

As expected, elevated concentrations of aTc led to increases in the abundance of DnaAcos (Fig. 3A). Furthermore, the obtained DnaAcos expression levels as function of aTc concentrations were

Downloaded from https://www.science.org at AMOLF on November 11, 2026

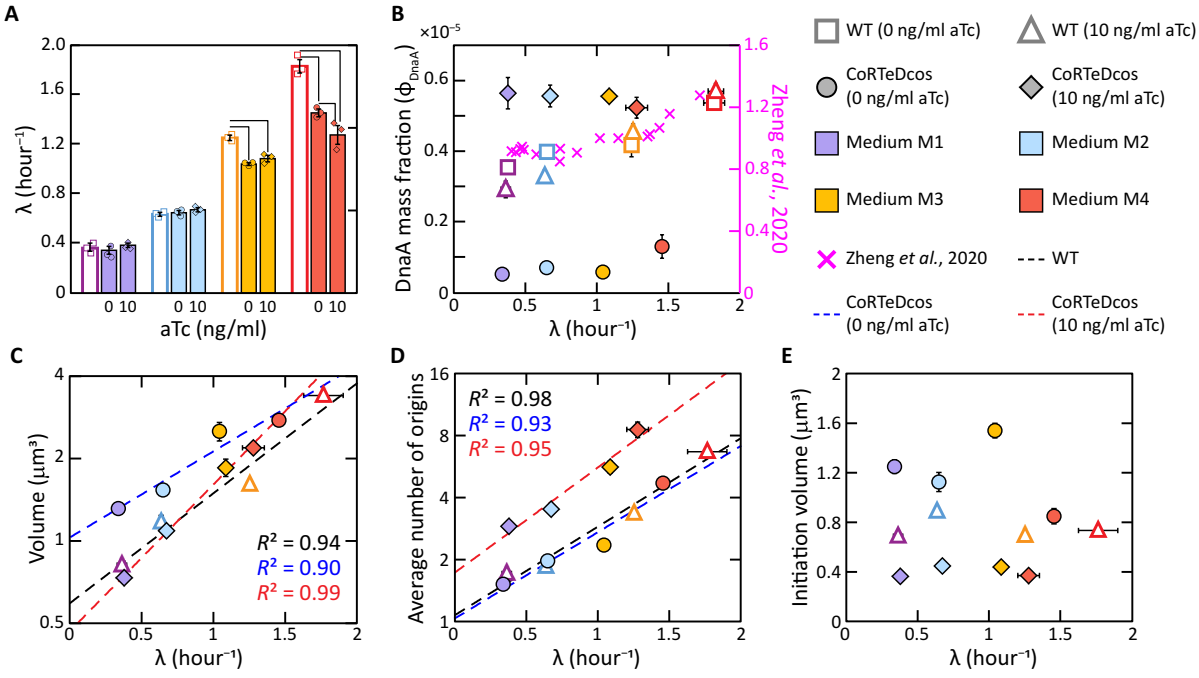


Fig. 2. Phenotypical characterization of *E. coli* CoRTeDcos. After balanced growth in turbidostat reactors, we characterized the (**A**) growth rate, (**B**) mass fraction of DnaA (ϕ_{DnaA}), (**C**) volume, (**D**) number of origins, and (**E**) volume of initiation of *E. coli* MG1655 (open symbols) and *E. coli* CoRTeDcos (filled symbols) in four different media (M1: purple, M2: blue; M3: yellow; M4: red) and two concentrations of aTc (0 and 10 ng/ml). Each bar or point is the average of three independent biological replicates (i.e., separate turbidostat cultivations), while the error bar indicates the SD. In (A), individual data points are plotted, and statistically significant differences (*t* test, $P < 0.05$) are indicated by the black lines. In (B), data extracted from Zheng *et al.* (*12*) are plotted for comparison. In (C) and (D), cellular parameters are plotted on semilog axes and exponential fits were applied to indicate relationships between growth rate and different parameters for either *E. coli* MG1655 (black line) or *E. coli* CoRTeDcos (blue line: 0 ng/ml; red line: 10 ng/ml). WT, wild type.

comparable between media M1 and M3, further validating the capacity of the coregulatory construct to maintain stable $\phi_{DnaAcos}$ across growth rates. The different concentrations of aTc all led to similar growth rates in the same medium (fig. S4A). The volume and number of origins of *E. coli* CoRTeDcos were considerably different at the same $\phi_{DnaAcos}$ across media [Fig. 3, B and C, see also fig. S4 (B and C) for media M2 and M4], further reinforcing the idea of the general growth law that these parameters are set by the specific nutrient availability (*7*, *12*, *46*). We also noticed an exponential decrease of cellular volume within the same medium at increasing $\phi_{DnaAcos}$ values (Fig. 3B), while the average number of origins increased exponentially (Fig. 3C). These tight correlations span a large range of DnaAcos protein levels, ultimately breaking down at the highest tested aTc concentrations. The anticorrelation between volume and number of origins was lost in medium M1 supplemented with 20 ng/ml of aTc, where both values increased. In medium M3, concentrations of 15 and 20 ng/ml caused an unexpected increase of cell volume and a decrease in the number of origins. On the other hand, the volume of initiation seemed to be independent of growth rate and uniquely determined by the abundance of DnaAcos (Fig. 3D and fig. S4D). More specifically, a single exponential relationship can explain the change in volume of initiation of *E. coli* CoRTeDcos caused by different $\phi_{DnaAcos}$ (Fig. 3D). The volumes of initiation of *E. coli* CoRTeDcos in medium M3 at 15 and 20 ng/ml of aTc emerged as outliers.

Last, we compared the values of volume of initiation of *E. coli* CoRTeDcos at different $\phi_{DnaAcos}$ with predictions coming from a titration model (*26*) and a titration-switch model (*26*). We also included predictions coming from the recently proposed titration-extrusion and titration-switch-extrusion models (*48*), where the nucleoid-associated protein H-NS facilitates replication initiation by extruding DnaA from the chromosome. To this end, we simulated the expression, titration, and/or interconversion of DnaA in the cell over time, together with the expression and effect of H-NS for models including extrusion (*48*). When model-specific conditions causing DNA replication initiation are met (e.g., saturation of titration sites in a titration model), the volume of initiation was recorded. The synthesis rate of DnaA was then systematically changed. For both predictions and experiments, values of volume of initiation were normalized to the average of all values in the same condition to obtain relative volumes of initiation. Relative DnaA expression levels were calculated in the same way. The simulations were performed for four different doubling times, similar to the ones experimentally obtained (i.e., 120, 60, 30, and 20 min). The experimental datasets were then compared to the predictions of the different models at the same doubling time via reduced chi-squared statistics (χ_ν^2) (see Materials and Methods for more details on the simulations and statistical analysis). We noticed that the experimental data resembled predictions coming from a pure titration model more closely ($\chi_\nu^2 \approx 20$; Fig. 4) and deviated more considerably from predictions coming from a titration-switch model (*26*, *48*) ($\chi_\nu^2 \approx 45$; fig. S5A) or the recently proposed titration-extrusion (*48*) ($\chi_\nu^2 \approx 71$; fig. S5B) and titration-switch-extrusion models (*48*) ($\chi_\nu^2 \approx 54$; fig. S5C). The values previously mentioned as outliers (i.e., 20 ng/ml of aTc in medium M1 and 15 and 20 ng/ml of aTc in medium M3) were also included in the statistical analysis, but the

Downloaded from https://www.science.org at AMOLF on November 11, 2026

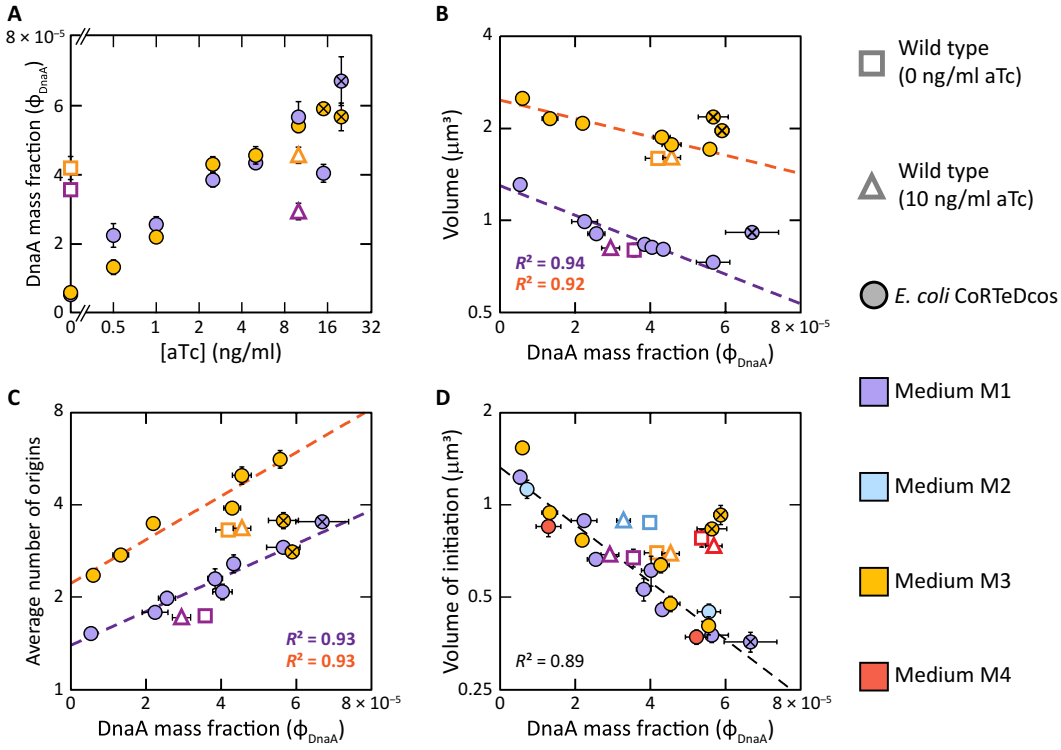


Fig. 3. The influence of the abundance of DnaAcos on volume, number of origins, and volume of initiation in *E. coli* CoRTeDcos. (**A**) Values of $\phi_{DnaAcos}$ at different concentrations of aTc. (**B**) Cell volume, (**C**) number of origins, and (**D**) volume of initiation per origin of *E. coli* CoRTeDcos (filled circles) are all correlated to $\phi_{DnaAcos}$. In (D), data coming from *E. coli* CoRTeDcos grown in media M2 and M4 are also presented. For other panels, data coming from media M2 and M4 are plotted in the Supplementary Materials (fig. S4, B and C). In all graphs, *E. coli* MG1655 values are shown for comparison (open symbols). Purple, blue, yellow, and red symbols represent data acquired from cells grown in media M1, M2, M3, and M4, respectively. The dashed lines are exponential fits of *E. coli* CoRTeDcos values. Crossed points represent the outliers excluded from the exponential fits. In (D), a single exponential trendline was used to fit data coming from all media. See the Supplementary Materials (fig. S4D) for individual trendlines for media M1 and M3. In all cases, cells grown in M1 with 20 ng/ml of aTc and in M3 with 15 and 20 ng/ml of aTc were deemed as outliers due to the discrepancy in the change in volume compared to the general trend. Cell volume plots where these conditions are also used are available in the Supplementary Materials (fig. S4E). All data points are the average of three independent biological replicates, and error bars represent the SD. In some cases, error bars are smaller than the symbols.

results did not change when excluding them (see data S1 related to fig. S5 for all χ_ν^2 values). Notably, a recent study altered the mRNA levels of wild-type *dnaA* and found that the relationship between volume of initiation and DnaA expression does not support a model based solely on initiator titration (*48*). We attribute the difference between this recent report and our study to the absence of DnaA interconversion in *E. coli* CoRTeDcos. We refrained from directly comparing the two datasets because changes in mRNA levels do not directly lead to the same changes at a protein level (*49*).

Notably, there were two conditions in which the behavior of *E. coli* CoRTeDcos differed from the trendline predicted by a titration system. First, cell populations grown in the absence of aTc, and thus with low DnaA concentrations (Figs. 2B and 3A), showed a lower volume of initiation than expected from simulations of the titration model (Fig. 4A). This difference might hint at additional unknown regulatory mechanisms stabilizing initiation. Furthermore, the absence of aTc was also associated with large-scale proteomic changes in *E. coli* CoRTeDcos compared to conditions where the inducer was present, hinting at a complex phenotype that cannot be easily explained via DnaAcos abundances alone (fig. S6). The second case of deviation from the predicted trend concerns the behavior of *E. coli* CoRTeDcos in medium M3 with high concentrations of aTc. We explain this phenomenon with the predicted instability of titration-based systems at high growth rates (Fig. 4B) (*26*, *27*). In nutrient-rich conditions leading to overlapping replication forks, the rate of new DnaA synthesis is higher than the rate at which new DnaA boxes are formed per origin (*25*, *26*). As a result, the available titration sites are quickly saturated, and the free DnaA concentration increases rapidly, causing an early initiation event. At this stage, the free DnaA concentration remains high due to the nutrient-imposed synthesis rate and one or more new replication rounds are rapidly reinitiated. With the progression of multiple replication forks, the total synthesis of titration sites, summed over all origins, becomes higher than DnaA synthesis rate. The resulting accumulation of a large titration power leads to prolonged periods of low free DnaA concentrations and no new initiation events. Each cell cycle thus exhibits multiple rounds of replication initiation, causing the initiation volume per origin to oscillate between a high and a low value (*26*, *27*). On the other hand, at lower growth rates, DnaA synthesis proceeds slower, and new DnaA boxes are formed quickly enough to maintain its free concentration below levels causing new initiation events (*26*). Rapid reinitiation of DNA replication is normally associated with lethal hyper-replicative stress (Fig. 1B) (*4*, *29*, *33*). In *E. coli* CoRTeDcos, the pressure against this stress possibly caused the selection of a mutation in DnaB. We hypothesize that the lower processivity of the helicase resulting from the M242I mutation (*41*) has a twofold function. First, a slower

Downloaded from https://www.science.org at AMOLF on November 11, 2026

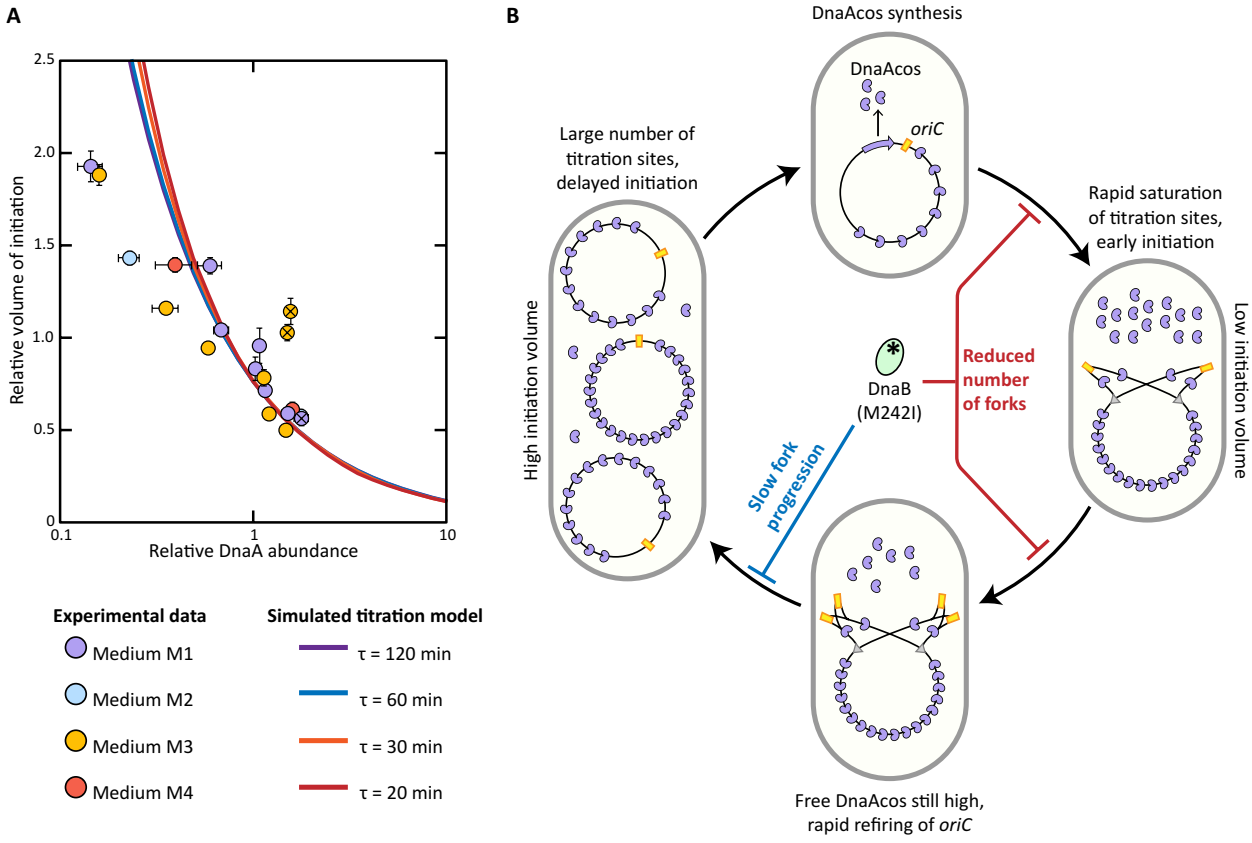


Fig. 4. Behavior and limitations of a titration-based control of DNA replication. (**A**) Comparison of the relationship between relative change in DnaA expression and relative change in volume of initiation from *E. coli* CoRTeDcos measurements (circles) and predictions of a titration model (smooth lines). Simulations were performed using a doubling time of 120 min (purple line), 60 min (blue line), 30 min (orange line), or 20 min (red line). Purple, blue, yellow, and red symbols represent data acquired from cells grown in media M1, M2, M3, and M4, respectively. Crossed points represent the outliers previously mentioned in Fig. 3. All data points are the average of three independent biological replicates, and error bars represent the SD. In some cases, error bars are smaller than the symbols. (**B**) The predicted instability of titration-based systems at high growth rates and concentrations of DnaAcos leads to cells oscillating between a low initiation volume (right) and a high initiation volume (left). We hypothesize that the M242I mutation in DnaB rescues the cell from lethal hyper-replicative stress by limiting initiations (red lines) and/or lowering fork collisions (blue line).

progression on the chromosome might reduce the chance of two forks colliding when a replisome is stalled, minimizing DNA damage. Second, the DnaB mutation can limit the total number of ongoing replication forks. DnaB is known to be present in few copies inside *E. coli* cells (*50*), and six monomers are needed to form a DNA helicase (*51*). For this reason, a slower processivity of the DNA helicase might lead to a longer turnover time before DnaB subunits become available to start a new round of replication, independently of whether DnaAcos already unwound *oriC*. Supporting this hypothesis, we observed that the origin/terminus ratio, estimated via mapping of sequencing reads (*52*), is higher in *E. coli* pre-CoRTeDcos than in *E. coli* CoRTeDcos (fig. S7A). This finding is in line with the potential role of DnaB(M242I) in indirectly reducing replication events in our final *E. coli* CoRTeDcos strain. The combination of these two effects might stabilize the system and allow *E. coli* CoRTeDcos to grow in all the tested conditions. However, cells might still be exhibiting oscillating replication initiations, and the type of measurements used here would only reflect population averages. A deeper analysis of *E. coli* CoRTeDcos at the single-cell level might also reveal unexpected, similar behaviors at growth rates not leading to overlapping replication forks at high $\phi_{DnaAcos}$. Our observations in medium M3 at the highest concentrations of inducer [i.e., higher volumes (Fig. 3B) and lower number of origins (Fig. 3C)] could then indicate that cells spend, on average, more time in the phase in which no replicative events take place.

E. coli CoRTeDcos proteome suggests hyper-replicative stress during fast growth

To obtain further evidence on the instability of titration-based systems during fast growth, we looked for changes in the proteome of *E. coli* CoRTeDcos indicative of a condition of hyper-replicative stress. Although there is no characterized proteome signature for this type of stress, the events eventually leading to cell death in these conditions are well known (Fig. 5A). Uncontrolled initiations of replication lead to several parallel forks accumulating on the chromosome. The quick depletion of the deoxynucleotide triphosphate (dNTP) pool in the cell then causes the replication forks to slow down and eventually arrest and/or collide (*53*, *54*). Moreover, the presence of reactive oxygen species (ROS) in the cell leads to the introduction of lesions in the nascent DNA (*55*). For these reasons, mutations lowering origin firing (*39*, *56*), increasing the available amount of dNTPs (*54*), or decreasing the presence of ROS (*40*, *55*) are known to rescue the cell from hyper-replicative stress. Hence, we investigated the proteome of *E. coli* CoRTeDcos for changes in the expression of proteins that would reduce initiation events [DiaA (*38*), DnaB (*38*), SeqA (*39*),

Downloaded from https://www.science.org at AMOLF on November 11, 2026

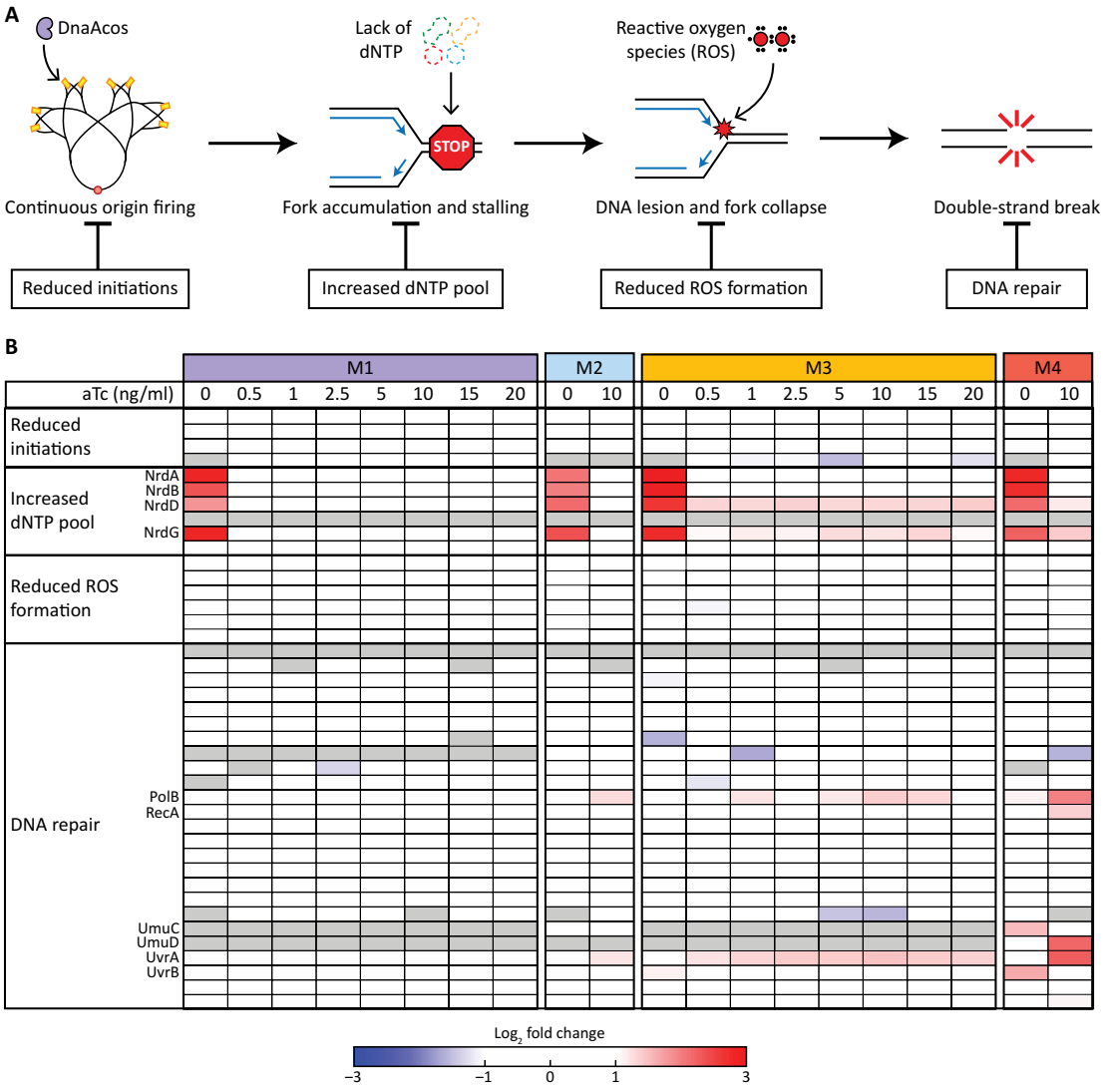


Fig. 5. *E. coli* CoRTeDcos undergoes replicative stress during fast growth. (**A**) Hyper-replicative stress caused by continuous origin firing leads to fork accumulation and stalling, ROS-mediated DNA lesions, and fork collapse. These events ultimately generate double-strand breaks in the chromosome of *E. coli* that, if not repaired, lead to cell death. Several proteins can suppress this lethal phenotype, by reducing the number of initiations, increasing the dNTP pool, reducing the formation of ROS, or repairing DNA. (**B**) Changes in production of sets of proteins involved in the different forms of rescue from hyper-replicative stress. For each cell in the heatmap, proteins produced with more than a twofold difference compared to wild type are mapped in gradients of either blue (underexpression) or red (overexpression). Proteins that could not be detected in more than two samples either in *E. coli* CoRTeDcos or in *E. coli* MG1655 are indicated in gray and were omitted from the analysis. Proteins with a more than twofold different production compared to the wild-type background are indicated in the figure. The complete list of proteins belonging to each group is available in data S1, together with their relative fold change.

and YfdQ (*56*)], increase the dNTP pool (Nrd proteins) (*39*, *53*, *54*), or reduce the formation of ROS (AtpAB, CydAB, Fre, and IscU) (Fig. 5B) (*40*). We also searched for changes in the synthesis of proteins associated with DNA repair mechanisms, as we argued that they could suggest the presence of DNA damage.

In the slowest tested growth conditions (medium M1, $\lambda \approx 0.37$ hour^{-1}), we noticed no proteome changes that could indicate an adaptation to replicative stress. With richer nutrient conditions and thus improved growth rates, we observed a progressively larger overexpression of proteins involved in dNTP synthesis and DNA repair. In medium M2 ($\lambda \approx 0.7$ hour^{-1}), the presence of aTc led to an increased abundance of two DNA repair proteins [PolB (*57*, *58*) and UvrA (*59*)]. In media promoting overlapping replication forks (i.e., M3 and M4), two additional proteins involved in DNA repair [UmuC (*60*, *61*) and UvrB (*59*)] were overproduced even in the absence of aTc. Increased levels of inducer and thus DnaAcos then further aggravated these proteome changes. In general, we observed a more abundant production of proteins involved in repairing DNA lesions and double-strand breaks [PolB (*57*, *58*), RecA (*62*), UvrABD (*59*), and UmuCD (*60*, *61*)]. The anaerobic ribonucleotide reductase protein NrdD and its activator protein NrdG were also among the proteins overexpressed upon induction of DnaAcos, despite the fact that all our cultivations were performed in aerobic conditions. A similar response has been previously reported in hyper-replicating mutants (*38*, *54*). The NrdA,

Downloaded from https://www.science.org at AMOLF on November 11, 2026

NrdB, NrdD, and NrdG proteins were also strongly overexpressed (between 3.6- and 8-fold) in the absence of aTc at all growth rates. The *nrdA* and *nrdD* operons are known to be part of the DnaA regulon (*63*, *64*), yet their activation or repression only partially depends on DnaA (*63*, *65*). It is thus possible that very low $\phi_{DnaAcos}$ (between 0.13 and 0.23 times the wild-type levels) contribute to elevated transcription of the *nrd* operons. We did not notice any major changes in expression that could indicate a reduction in DNA replication initiation or a lower formation of ROS. Moreover, the observed changes were not attributable to the presence of aTc alone, as evident from the analysis of wild-type *E. coli* proteomes (fig. S6). To account for the possibility that some of the observed changes could be due to a difference in growth rate, we compared the proteomes of *E. coli* CoRTeDcos in medium M4 with 10 ng/ml of aTc ($\lambda = 1.28 \pm 0.08$ hour^{-1}) with the one of *E. coli* MG1655 in medium M3 ($\lambda = 1.25 \pm 0.02$ hour^{-1}). We obtained a similar set of overexpressed proteins, indicating that the implemented form of DNA replication control is likely responsible for the observed changes (fig. S8). To understand whether the observed stress caused replication fork arrest, we performed marker frequency analysis (*52*) in *E. coli* CoRTeDcos grown in media M3 and M4. Replication forks progressing normally are known to generate a linear decay in the $\log_2$-transformed marker frequency from *oriC* to terminus of replication. Conversely, forks stalling or collapsing at nondefined chromosomal positions lead to a nonlinear increase in marker frequency toward *oriC* (*66*). Therefore, we fitted the marker frequency data on each replichore to both a single straight line, indicative of normal progression, and a broken-stick model, indicative of fork arrest. We then assessed which model best fitted the replicative profiles of our strains (see Materials and Methods for more details). In all tested conditions, our analysis suggested that *E. coli* CoRTeDcos replication forks proceed normally without substantial arrest (fig. S7B).

Overall, the proteome analysis of *E. coli* CoRTeDcos seems to indicate the presence of replicative stress during faster growth at almost all inducer concentrations, despite the mitigating effect of the DnaB(M242I) mutation. Moreover, they suggest that this type of stress can be present even in cells that do not lose the typical anticorrelation between cell volume and the number of origins. Still, our marker frequency analysis seems to indicate that replication forks proceed mostly unhindered in *E. coli* CoRTeDcos, likely due to the differential expression of certain proteins. Specifically, we hypothesize that a larger abundance of Nrd proteins can increase the dNTP pool and minimize fork stalling, while the DNA repair machineries can efficiently resolve potential DNA damage.

DISCUSSION

In this study, we established a titration-based control of DNA replication in *E. coli* CoRTeDcos with only minimal genetic modifications and the aid of selective pressure. This result was achieved (i) by replacing the ATP/ADP-controlled wild-type DnaA initiator with an "always-active" variant DnaAcos and (ii) by selection of a single amino acid substitution in the helicase protein DnaB. The use of a coregulatory construct further allowed us to probe the behavior and limits of the system at different concentrations of DnaAcos (Figs. 2 and 3). Titration of DnaAcos relied entirely on the native amount of DnaA boxes, further confirming the capacity of *E. coli* chromosome to sequester the initiator protein (*25*). We obtained a titration-based system recreating the phenomenon of stable volumes of initiation across growth rates (Figs. 3 and 4). In *E. coli* CoRTeDcos, the specific value of volume of initiation can then be controlled by inducing the $P_{LtetO\text{-}1}$ promoter via aTc.

On top of providing insights into the capacity and limit of DnaA titration in replication control, it is interesting to look at our results from an evolutionary perspective. Initiator titration has been proposed as the possible control mechanism of slow-growing ancestors of *E. coli* (*27*, *67*). In this hypothesis, the interconversion between DnaA-ATP/DnaA-ADP was adopted later in this bacterium evolutionary trajectory to allow doubling times shorter than the time needed for chromosome replication. In line with this idea, we previously reported a shared genomic configuration favoring the titration of DnaA among most *E. coli* strains (*25*). Here, we elaborate on these previous studies by showing that our *E. coli* CoRTeDcos strain seems to be more stable during slow growth. In this condition, the volume of initiation maintained an exponential inverse relationship with $\phi_{DnaAcos}$ (Fig. 3), and we did not observe any change in protein expression hinting at the presence of replicative stress (Fig. 5). On the other hand, growth conditions promoting overlapping replication forks caused atypical behaviors that can be reconciled with hyperreplicative stress. Several proteins involved in nucleotide synthesis and DNA repair pathways were always overproduced (Fig. 5), and high levels of DnaAcos caused a counterintuitive increase in volume of initiation (Fig. 4). We speculate that this same instability served as evolutionary pressure leading to the adoption of the DnaA interconversion mechanism in *E. coli* ancestors. It is important to note that our conclusions are based on population averages that inevitably mask any single-cell behavior or variation. For this reason, we cannot directly observe the occurrence of multiple initiation events within the same cell division cycle predicted by the titration model during regimes of overlapping replication. Notably, unstable regimes could also emerge during slow growth in the absence of overlapping replication forks and at high $\phi_{DnaAcos}$ but remain undetectable by our approach. In the future, studying *E. coli* CoRTeDcos in microfluidic cultivation settings (*6*, *68*) could shed light on the intricacies of its regulation strategy at a single-cell level and further help in tuning the system. Moreover, the use of fluorescent reporters of DNA damage (*69*) could be used in the same single-cell settings to further assess the system stability and fine-tune it in different growth conditions.

Last, we believe that our results may be useful in the field of synthetic cells. Specifically, the creation of a functional synthetic cell must meet the fundamental requirement of one replication event per cell division (*70*). If not, the cellular DNA content would not remain constant throughout generations, continually increasing until death (*70*). This requirement is already not trivial in natural cells (*71*), but its recreation faces further technical limitations in the field of synthetic cells. Because of the complexity of building synthetic cells with a bottom-up approach, the use of minimal systems is generally preferred in the reconstitution of cellular process (*70*, *72*). Hence, simple replication machineries and control strategies are preferred for bottom-up synthetic cells. The design criteria used here can, in principle, be repurposed for initiator proteins different from DnaA, to allow a simple control strategy for other, more minimal replication machineries. For instance, the replicative machinery derived from bacteriophage ϕ29 (*73*) has been the system of choice in the study of DNA replication for synthetic cells in the past years (*70*, *74*). Engineering high- and low-affinity binding sites for the terminal DNA binding protein (p3) would thus yield a titration-based control mechanism that only requires addition of binding motifs in specific sections

Downloaded from https://www.science.org at AMOLF on November 11, 2026

of the future synthetic cell chromosome (*75*). Notably, the high processivity of the ϕ29 DNA polymerase protein p2 (*76*) might still lead to unviable cells at higher growth rates, where a slower replication machinery (Fig. 1) and DNA repair mechanisms (Fig. 5) seem to be needed. Because of the field's tendency to prefer minimal systems (*70*), the metabolic routes implemented in the final synthetic cell might not generate growth rates high enough for our system to become unstable. Still, evolution-based methods for the implementation of modules in synthetic cells (*77*) could be exploited to obtain a ϕ29 replication machinery optimizing fork speed and stability. The resulting system would thus accomplish the goal of streamlined and growth-coupled DNA replication initiation, without the input of additional ATP (*13*) or eukaryotic-like complex genetic architectures (*78*).

MATERIALS AND METHODS

Bacterial strains and growth conditions

A list of bacterial strains used in this study is provided in the Supplementary Materials (table S1). *E. coli* DH5α (NEB) was used for general plasmid propagation and standard molecular techniques. The wild-type *E. coli* MG1655 and the mutant strain *E. coli* CoRTeDcos were used for all phenotypical characterization experiments.

E. coli CoRTeDcos was routinely propagated at 30° or 37°C and 200 rpm in M9 liquid medium supplemented with either 22 mM glycerol or 22 mM glucose. All other *E. coli* strains were routinely propagated at 30° or 37°C and 200 rpm in LB liquid medium. For constant density cultivations, four different liquid media were used (M1 to M4), yielding growth rates ranging from 0.4 to 1.8 $hour^{-1}$. Media M1, M2, and M3 were based on M9 medium, supplemented with either glycerol or glucose as carbon source and eventually different amounts of amino acids. Medium M4 was a tryptic soy broth. Complete medium composition is available in the Supplementary Materials (table S2). All strains were cultivated at 37°C in M1, M2, M3, or M4 medium, eventually supplemented with aTc. Media were eventually supplemented with agar (15 g/liter) to obtain solid media and with antibiotics for strain selection or plasmid propagation [kanamycin (50 mg/liter), ampicillin (100 mg/liter), and chloramphenicol (25 mg/liter)]. Phosphate-buffered saline (PBS) solution (137 mM NaCl, 2.7 mM KCl, 10 mM Na_2HPO_4, and 1.8 mM KH_2PO_4) was used to wash cells during sample preparation.

Plasmid and linear knock-in fragment construction

A list of all plasmids used in this study is provided in the Supplementary Materials (table S3). The CoRTeDcos mutation was introduced in *E. coli* MG1655 using the pSC020 plasmid system, containing the λ-red recombineering system and the Cre recombinase (*79*). To obtain the linear fragment for recombination while avoiding toxicity of DnaAcos, the CoRTeDcos locus was split into two fragments, each cloned in a separate plasmid. The pCoRe-T plasmid was based on a pUC19 backbone and contained, in order, a chloramphenicol resistance cassette flanked by *lox66* and *lox71* sites (*80*), the TetR repressor under the control of the $P_{LtetO-1}$ promoter, and a BsaI restriction site generating a 5′-TCAG sticky end. The pCoRe-Dcos plasmid was based on a pUC19 backbone and contained, in order, a BsaI site generating a 5′-AGTC sticky end, the *dnaAcos* gene, and a kanamycin resistance cassette flanked by *lox66* and *lox71* sites (*80*). The DnaAcos gene was chemically synthesized (BG22166). To obtain the linear recombination fragment, first a polymerase chain reaction (PCR) reaction was performed on pCoRe-T with primers BG22660 and BG20764 and on pCoRe-Dcos with primers BG21406 and BG22661. The two fragments were then purified and mixed in equimolar amounts together with BsaI (NEB) restriction enzyme and T4 DNA ligase (NEB) in CutSmart reaction buffer (NEB). The reaction mixture was incubated at 37°C for 1 hour, before being heated up to 80°C for 5 min to inactivate the enzymes. Five microliters of reaction was then used as a PCR template with primers BG22660 and BG22661 to amplify the full recombination fragment generated in the previous restriction-ligation reaction. Primer BG22660 contained an overhang with 50 bp of homology to positions 3883943-3883993 of *E. coli* MG1655 genome (upstream of the P_{dnaA} promoter); primer BG22661 contained an overhang with 50 bp of homology to positions 3882292-3882342 of *E. coli* MG1655 genome (downstream of *dnaA* and into the *dnaN* gene).

DNA fragments were amplified by PCR using Q5 High-Fidelity DNA Polymerase (NEB) following the manufacturer's instructions. Specific oligonucleotides and synthetic DNA were designed and synthesized (IDT) to introduce proper overhangs for assembly. The sequences of primers and synthetic DNA used in this study are provided in the Supplementary Materials (table S4). Plasmid assembly was performed using NEBuilder HiFi DNA Assembly Master Mix (NEB).

Transformation procedure and creation of *E. coli* CoRTeDcos

For all transformation procedures, cells were made electrocompetent and transformed through electroporation as previously described (*25*). The pCoRe-T and pCoRe-Dcos plasmids were transformed and propagated in *E. coli* DH5α. The pSC020 plasmid (*81*), containing the λ-red recombination system and the Cre recombinase, was transformed in *E. coli* MG1655. To create *E. coli* CoRTeDcos, electrocompetent *E. coli* MG1655 cells carrying the pSC020 plasmid were transformed with 200 ng of linear CoRTeDcos fragment, plated in solid M1 medium supplemented with kanamycin, chloramphenicol, and ampicillin, and incubated at 30°C. Insertion of the coregulatory construct was confirmed first by colony PCR using primers BG22467 and BG22496 and then by Sanger sequencing of the locus. Correct colonies were propagated in solid M1 medium supplemented with ampicillin and 1 mM isopropyl-β-D-thiogalactopyranoside to induce expression of Cre recombinase and incubated at 30°C. Colonies that lost kanamycin and chloramphenicol resistances were propagated in solid M1 medium at 37°C to promote loss of the pSC020 plasmid. After screening for colonies sensitive to ampicillin, whole-genome sequencing was performed to ensure that the coregulatory construct was the only source of DnaA in the chromosome of *E. coli*. The final strain *E. coli* CoRTeDcos emerged during prolonged incubation of the initial mutant strain in M3 medium supplemented with aTc (10 ng/ml). Whole-genome sequencing was performed to identify the *dnaB* mutation selected for in *E. coli* CoRTeDcos (table S5).

Turbidostat cultivation of cell cultures and growth rate characterization

We used constant-density cultivation inside turbidostat reactors to obtain *E. coli* cultures in balanced growth. *E. coli* strains were first grown overnight in 5 ml of M1 or M3 medium at 37°C and 180 rpm. The densely grown culture was then used to start a turbidostat cultivation using the Pioreactor platform (Pioreactor 40 ml v1.0; software version 25.5.22; Pioreactor Inc., https://pioreactor.com). Experiments were started according to the manufacturer's instructions for fluidic lines, electrical connections, and user interface. Cultures were started at an optical density at 600 nm (OD_{600nm}) of 0.05 in media M1 to

Downloaded from https://www.science.org at AMOLF on November 11, 2026

M4, supplemented with aTc appropriately. Default settings were used for frequency of optical density measurements; temperature was set to 37°C, and stirring was set to 700 rpm. The target optical density was set to OD_{600nm} of 0.3, and the media reservoir was filled with the same medium as in the cultivation chamber. Cultivation medium was pumped in the vessel from the reservoir to maintain a constant optical density. Cells were balanced in exponential growth at the target optical density for at least 10 generations before harvesting. Last, cells were harvested in different amounts for downstream processing. Three biological replicates were obtained for every strain and condition by performing independent turbidostat cultivations.

For each turbidostat cultivation, we estimated growth rate (λ) using the dilution rate (D). The total volume ($V_{SteadyState}$) and time ($t_{SteadyState}$) spent at the steady-state optical density were used to calculate the flow rate $F = \frac{V_{SteadyState}}{t_{SteadyState}}$. F was then used together with the cultivation volume ($V_{Culture} = 20$ ml) to calculate dilution rate and thus growth rate, following $\lambda = D = \frac{F}{V_{Culture}}$. Doubling times (τ) were obtained from growth rates measurements.

In microplate reader growth assays, cells coming from an overnight culture were used to inoculate a medium containing different aTc concentrations at an initial OD_{600nm} of 0.05. One hundred fifty microliters of inoculated medium was topped with 50 μl of mineral oil to prevent evaporation during the growth experiment. Growth of the different strains was assessed in each condition in three biological replicates. The medium used for the overnight culture was the same medium used in the final microplate reader assay, with the difference that cells were always propagated in the absence of aTc overnight. The two media used were both based on M9, either supplemented with 20 mM of acetate (slow growth) or with 20 mM of glucose and RPMI amino acids (fast growth). Growth was then monitored by absorbance at 600 nm using a Synergy H1 microplate reader (BioTek) at 37°C and orbital shaking either over 48 hours for slow growth or 20 hours for fast growth experiments. A previously published MATLAB script (*82*) was used to estimate growth rate from each growth curve.

Proteomic analysis

To perform proteomics, 10 ml of turbidostat cultures of *E. coli* strains in different growth conditions was harvested. Cells were then washed in PBS before being pelleted, and bacteria were lysed with 100% trifluoracetic acid (TFA) according to the SPEED protocol (*83*) with slight adaptations (*84*). Briefly, 25 μl of 100% TFA was added to the pellet, incubated for 5 to 7 min at 55°C, and neutralized with 225 μl of 2 M tris. Protein concentration from lysed samples was quantified via Bradford assay. Fifty micrograms of total protein amount per sample was reduced and alkylated [9 mM tris(2-carboxyethyl)phosphine and 40 mM chloroacetamide]. Protein digestion was performed with a trypsin (Roche)–to–protein ratio of 1:50 overnight at 37°C. Samples were desalted by solid-phase extraction (C18) and stored after lyophilization at −80°C. Peptides were analyzed on a Vanquish Neo UHPLC (microflow configuration; Thermo Fisher Scientific) coupled to an Orbitrap Exploris 480 mass spectrometer (Thermo Fisher Scientific). Around 25 μg of peptides was applied directly onto a commercially available Acclaim PepMap 100 C18 column (2-μm particle size, 1 mm ID by 150 mm, 100-Å pore size; Thermo Fisher Scientific) and separated using a 60-min linear gradient ranging from 3 to 28% solvent B [0.1% FA and 3% dimethyl sulfoxide (DMSO) in ACN] in solvent A (0.1% FA and 3% DMSO in high-performance liquid chromatography–grade water) at a flow rate of 50 μl/min. The mass spectrometer was operated in data-independent acquisition (DIA) mode. MS1 full scans [360 to 1300 mass/charge ratio (m/z)] were acquired with a resolution of 120,000, an AGC target value of 1×10^6, and a maximum injection time of 50 ms. The cycle time was set to 3 s. MS2 scans (200 to 1800 m/z) were acquired over 40 DIA segments with widths adjusted to the precursor density [see supplementary table 8 in (*85*)]. The scan resolution in the Orbitrap was set to 15,000 with an AGC target value of 1×10^5 and a maximum injection time of 22 ms. The HCD collision energy was set to 30%. The mass spectrometric raw files were analyzed with DIA-NN (*86*) (version 1.8) using the UniProt reference FASTA file for *E. coli* K-12 (UP000000625, download 04 June 2023, 4403 protein entries) appended with common contaminants. FASTA digest for library-free search and deep learning–based spectra was enabled. N-term M excision, C carbamidomethylation, and Ox(M) were activated. The peptide length range was set from 7 to 30, precursor charge ranged from 2 to 6, precursor m/z ranged from 360 to 1300, and fragment ion m/z ranged from 200 to 1800. Usage of isotopologues and match-between runs were enabled. Precursor FDR was set to 1%. All other parameters were kept as default. The DIA-NN main report table "report.pg_matrix.tsv" was processed with the R-script DIAgui (*87*), to obtain intensity-based protein quantification values (iBAQ intensities) (*88*) for the determination of protein mass fractions, as well as label-free quantification values (MaxLFQ intensities) (*89*) for relative protein quantification. Further processing was carried out with the in-house proteomic analysis tool "baybiomsCruncher" (https://github.com/nava20ir/baybiomsCruncher) (*90*). This processing included filtering proteins for being quantified in all three replicate measurements of at least one experimental condition, as well as imputation of missing values by replacement with random values drawn from a normal down-shifted distribution (width = 0.3, downshift = 1.8). Protein mass fractions of DnaA variants in the proteome of *E. coli* MG1655 and *E. coli* CoRTeDcos were calculated by dividing the iBAQ value of DnaA for the summed iBAQ values of all detected proteins in a given sample. Ribosome fractions (ϕ_R) were obtained by dividing the sum of the iBAQ value of all proteins associated with ribosomes for the summed iBAQ values of all detected proteins inside a given sample. To gain insights into the presence of hyper-replicative stress, MaxLFQ intensities of relevant proteins in *E. coli* CoRTeDcos were compared to the wild-type intensities. Only proteins that could be detected in at least two of the three biological replicates in both *E. coli* CoRTeDcos and *E. coli* MG1655 samples were considered. Protein fold changes relative to the wild type were used to generate a heatmap with a custom-made MATLAB script.

Cell size measurements

Cell size measurements were estimated via phase-contrast microscopy. Three milliliters of turbidostat cultures of *E. coli* was washed once with PBS and then resuspended in 10 μl of PBS in an Eppendorf tube. One to 2 μl of the final cell suspensions was immobilized on agarose pads (PBS supplemented with 1.5% agarose) on microscopy glass slides. Phase contrast images were acquired with an ECLIPSE Ti2 microscope (Nikon) equipped with a 100× immersion oil objective (numerical aperture = 1.4). Cells in the microscopic images were segmented using Omnipose (*91*), yielding cell masks. A custom-written Python script was used to extract values for length and width in pixels of each identified cell from the cell masks. The camera pixel size (49.4 nm × 49.4 nm) was used to generate the corresponding measurements in micrometers. The rod shape of *E. coli* was approximated to a cylinder with a

Downloaded from https://www.science.org at AMOLF on November 11, 2026

hemisphere at each pole, and the volume was estimated as $V = \pi\left(\frac{W}{2}\right)^2(L-W) + \frac{4}{3}\pi\left(\frac{W}{2}\right)^3$, using the obtained length (L) and width (W). In general, thousands of cells per replicate were used; exact numbers are reported in the Supplementary Materials (table S6).

Characterization of C period

In *E. coli* cultures undergoing steady-state growth, the relative frequency of two genomic loci depends on the C period, their relative distance, and the doubling time (*7*, *12*, *92*). To estimate the length of C period, digital PCR was used to estimate the relative abundance of origins and termini of replication. To this end, 5 ml of turbidostat cultures of *E. coli* was washed with PBS before being pelleted. Genomic DNA was extracted using the DNeasy Blood & Tissue Kit (QIAGEN) and eluted in Milli-Q water. Genomic DNA concentration was assessed using Qubit dsDNA BR Assay Kit (Invitrogen). All samples were then diluted to a concentration of 5 ng/μl, before being diluted an additional 200 times. Two microliters of the resulting genomic DNA solution was then used as input in digital PCR reactions. Each reaction was performed with QIAcuity EvaGreen Mastermix (QIAGEN) in a 12-μl reaction, using a QIAcuity Digital PCR System (QIAGEN). Previously reported (*7*) primer pairs were used to measure abundance of *oriC* (primers SJO416 and SJO417) and *ter* (primers SJO432 and SJO433). The C period was then obtained as $C = \tau \log_2\left(\frac{n_{oriC}}{n_{ter}}\right)$, where $\frac{n_{oriC}}{n_{ter}}$ refers to the relative abundance of the origin of replication and the terminus as obtained through digital PCR, and τ refers to the culture doubling time, obtained from the growth rates from turbidostat cultivation.

Flow cytometry estimation of genome equivalents

To perform flow cytometry, 2 ml of turbidostat cultures of *E. coli* was first added to 18 ml of ice-cold 70% (v/v) ethanol and allowed to fix at 4°C for at least 12 hours and for a maximum of 14 days (*93*). Cells were washed once with PBS and then resuspended in 1 ml of PBS in an Eppendorf tube. Ten microliters of the resulting cell suspension was stained with 2 μl of 100x Quant-iT PicoGreen dsDNA reagent (Invitrogen) in 25% DMSO (ratio of 1:1). The cells were incubated together with the nucleic acid dye for at least 90 min at room temperature in the dark. Last, 200 μl of PBS was added to the samples. All flow cytometry analyses were performed with a CytoFLEX (S) (Beckman Coulter Life Sciences) and the CytExpert software. For each sample, forward and side scatter measurements were obtained, together with emission filtered with a 530/30-nm transmission filter for DNA content measurement (B525-H channel, gain = 40). PicoGreen-stained particles were deemed to be bacterial cells, and at least 100,000 of these events were collected per sample. The DNA content of cell populations was represented as a histogram versus fluorescence on the green channel. *E. coli* MG1655 cells grown in M1 and subjected to run-out replication [cephalexin (30 μg/ml) and rifampicin (300 μg/ml)] were used to quantify the fluorescence intensity of one copy of *E. coli* chromosome as previously described (*25*, *93*). The value obtained in this way was used to convert fluorescence intensity of experimental samples to genome equivalents. An example of the used gating strategy is available in the Supplementary Materials (fig. S9).

Characterization of the number of origins and volume of initiation

Theoretical analysis (*7*) established a mathematical relationship between the length of the D period, the average genome equivalents ($\overline{G}$), the length of the C period, and the doubling time. Using this relationship and measured cellular parameters, the time of the cell cycle was obtained as $\tau_{cyc} = C + \tau \log_2\left[\frac{C\cdot\overline{G}\cdot\ln_2}{\tau\cdot\left(2^{\frac{C}{\tau}}-1\right)}\right]$. From here, the number of origins of the population (n_{oriC}) was estimated as $n_{oriC} = 2^{\frac{\tau_{cyc}}{\tau}}$. The volume of initiation (V^*) was estimated as $V^* = \frac{1}{\ln 2}\cdot\frac{\overline{V}}{n_{oriC}}$ (*7*, *46*), where $\overline{V}$ is the average cellular volume of the population.

Simulations of titration, switch, and extrusion models

To assess what theoretical model best fits our observations, we compared our experimental data with simulations of DNA replication in *E. coli* cells. To this end, we used a set of previously generated MATLAB scripts (*48*) (https://github.com/BaiYangBqdq/dynamics_of_biomass_DNA_coordination/tree/main), based on theoretical works performed by other studies (*24*, *26*) or by the same authors (*48*). Briefly, the scripts simulate the expression, titration, and/or interconversion of DnaA in the cell over time, together with the expression and effect of H-NS for models including extrusion. At every time step, the cell volume grows according to growth rate, the number and state of DnaA proteins (bound versus free; ATP-bound versus ADP-bound) are updated, and model-specific parameters are compared to critical values that would trigger replication initiation. Every time the critical condition is reached, an initiation event is recorded, and the relative initiation mass is saved. The simulation was repeated for a range of DnaA expression levels by varying the DnaA synthesis rate and the cell doubling time. In this way, we generated predictions on the change in volume of initiation across different DnaA expression levels and growth conditions using a titration model, a titration-switch model, a titration-extrusion model, or a titration-switch-extrusion model. Because of the inability of DnaAcos to bind nucleotides (*29*, *32*, *33*), we did not compare the experimental data with simulations of a switch-only model. We used the same value of the original work for all the parameters (see table S7 in the Supplementary Materials for the complete list), with the exception of the doubling time. The doubling time value was set to 20, 30, 60, or 120 min to approximate our experimental conditions. From our proteomic data, we observed that levels of the nucleoid-associated protein H-NS were roughly constant across the tested conditions. Therefore, we did not change the H-NS synthesis rate parameter when varying the cell doubling time. We refer to the original works for in depth mathematical derivations of the biological models (*24*, *26*, *48*) and explanation of the scripts (*48*). For both experimental and simulated data, the values of volume of initiation were normalized to the average of all values obtained in the same condition (i.e., the same medium for experimental data and same doubling time parameter for simulations) to obtain the relative volume of initiation. The relative DnaA values were obtained in the same way, starting from either $\phi_{DnaAcos}$ for experimental data or DnaA expression rate for simulations. The values of relative volume of initiation and relative DnaA obtained from the simulation were fitted to a trendline ($R^2 > 0.9$), and the obtained equations were used to estimate values of relative volume of initiation at different values of relative DnaA expression. Reduced chi-squared statistics (χ_ν^2) was then used to identify how closely the experimental values resembled the predictions of the different models. The reduced chi-squared statistics was calculated as $\chi_\nu^2 = \frac{\sum\frac{(O_i-P_i)^2}{\sigma_{eff,i}}}{\nu}$, where O_i and P_i are experimental and predicted values, respectively, at the same relative DnaA value,

Downloaded from https://www.science.org at AMOLF on November 11, 2026

$\sigma_{\text{eff},i}$ is the expected variance, and ν are the degrees of freedom. The expected variance was calculated as $\sigma_{\text{eff},i} = \sigma_{V^*}{}^2 + \left[\sigma_{\phi_{\text{DnaAcos}}} \cdot f'(x_i)\right]^2$, where σ_{V^*} is the experimentally obtained SD of the volume of initiation, $\sigma_{\phi_{\text{DnaAcos}}}$ is the experimentally obtained SD of the relative ϕ_{DnaAcos}, and $f'(x_i)$ is the slope of the trendline used to fit the predicted values at that specific value of relative ϕ_{DnaAcos}. The degrees of freedom were calculated as $\nu = N - k$, where N is the total number of experimental values and k is the total number of parameters of the equations used to fit the predicted values across doubling times. The model leading to the lowest χ^2_ν was considered as the one best describing the experimental observations. All experimental points were used in estimating the lowest χ^2_ν value, including the ones identified as outliers during the analysis of the behavior of *E. coli* CoRTeDcos in media M1 and M3 and different aTc concentrations. The statistical analysis was also repeated excluding the outliers, with no changes in outcome.

Characterization of replication fork progression via marker frequency analysis

We performed marker frequency analysis to assess the presence of replication fork attrition. Twenty milliliters of turbidostat *E. coli* cells was pelleted and washed first in PBS and then in Zymo DNA/RNA Shield before being pelleted again. The cell pellet was then sent to Plasmidsaurus for long-read whole-genome sequencing using Oxford Nanopore Technology, yielding a final coverage of ~50 to 80×. Minimap2 (v. 2.30) (*94*) and SAMtools (v. 1.22.1) (*95*) were used for read alignment and coverage depth assessment, using *E. coli* MG1655 as the reference genome (identifier NC_000913.3). A custom-made MATLAB script was then used to assess the marker frequency starting from the coverage depth assessment. The values obtained were binned in windows of 5000 bp, normalized for the total read count of the terminus region, and then converted to $\log_2$ space. For visualization purposes, genomic coordinates were expressed as distance from *oriC* for each replichore, yielding a normalized x axis spanning from −1 to 1 and centered at *oriC*. Marker frequency profiles were visualized using a moving average of 60 bins. During normal replication fork progression, the $\log_2$-transformed marker frequency decreases linearly from *oriC* to *ter*. On the other hand, fork attrition signatures often appear as an initial downward slope, followed by a more horizontal trend. Therefore, we analytically compared a single linear fit against a continuous piecewise (broken-stick model). The best-fitting model was assessed using Akaike information criterion and plotted on top of the marker frequency plot. The approach was validated on previously deposited deep sequencing reads coming from an *E. coli* strain producing nonlinear marker frequency profiles (Sequence Read Archive project ID: PRJNA738450, sample ID: SAMN19728937, run ID: SRR14828588) (fig. S7C) (*96*).

Supplementary Materials

The PDF file includes:
Figs. S1 to S9
Tables S1 to S7
Legends for data S1

Other Supplementary Material for this manuscript includes the following:
Data S1

REFERENCES

1. R. Ohbayashi, S. Hirooka, R. Onuma, Y. Kanesaki, Y. Hirose, Y. Kobayashi, T. Fujiwara, C. Furusawa, S.-Y. Miyagishima, Evolutionary changes in DnaA-dependent chromosomal replication in cyanobacteria. *Front. Microbiol.* **11**, 786 (2020).
2. J. P. Erzberger, M. L. Mott, J. M. Berger, Structural basis for ATP-dependent DnaA assembly and replication-origin remodeling. *Nat. Struct. Mol. Biol.* **13**, 676–683 (2006).
3. A. C. Leonard, P. Rao, R. P. Kadam, J. E. Grimwade, Changing perspectives on the role of DnaA-ATP in orisome function and timing regulation. *Front. Microbiol.* **10**, 2009 (2019).
4. L. A. Simmons, A. M. Breier, N. R. Cozzarelli, J. M. Kaguni, Hyperinitiation of DNA replication in *Escherichia coli* leads to replication fork collapse and inviability. *Mol. Microbiol.* **51**, 349–358 (2004).
5. C. Fernandez-Fernandez, D. Gonzalez, J. Collier, Regulation of the activity of the dual-function DnaA protein in Caulobacter crescentus. *PLOS ONE* **6**, e26028 (2011).
6. M. Wallden, D. Fange, E. G. Lundius, Ö. Baltekin, J. Elf, The synchronization of replication and division cycles in individual *E. coli* cells. *Cell* **166**, 729–739 (2016).
7. F. Si, D. Li, S. E. Cox, J. T. Sauls, O. Azizi, C. Sou, A. B. Schwartz, M. J. Erickstad, Y. Jun, X. Li, S. Jun, Invariance of initiation mass and predictability of cell size in *Escherichia coli*. *Curr. Biol.* **27**, 1278–1287 (2017).
8. W. D. Donachie, Relationship between cell size and time of initiation of DNA replication. *Nature* **219**, 1077–1079 (1968).
9. S. Cooper, C. E. Helmstetter, Chromosome replication and the division cycle of *Escherichia coli* Br. *J. Mol. Biol.* **31**, 519–540 (1968).
10. C. E. Helmstetter, DNA synthesis during the division cycle of rapidly growing *Escherichia coli* B/r. *J. Mol. Biol.* **31**, 507–518 (1968).
11. T. O. Boesen, G. Charbon, H. Fu, C. Jensen, M. Sandler, S. Jun, A. Løbner-Olesen, Dispensability of extrinsic DnaA regulators in *Escherichia coli* cell-cycle control. *Proc. Natl. Acad. Sci. U.S.A.* **121**, e2322772121 (2024).
12. H. Zheng, Y. Bai, M. Jiang, T. A. Tokuyasu, X. Huang, F. Zhong, Y. Wu, X. Fu, N. Kleckner, T. Hwa, C. Liu, General quantitative relations linking cell growth and the cell cycle in *Escherichia coli*. *Nat. Microbiol.* **5**, 995–1001 (2020).
13. T. Katayama, K. Kasho, H. Kawakami, The DnaA cycle in *Escherichia coli*: Activation, function and inactivation of the initiator protein. *Front. Microbiol.* **8**, 2496 (2017).
14. T. Katayama, S. Ozaki, K. Keyamura, K. Fujimitsu, Regulation of the replication cycle: Conserved and diverse regulatory systems for DnaA and *oriC*. *Nat. Rev. Microbiol.* **8**, 163–170 (2010).
15. K. Fujimitsu, T. Senriuchi, T. Katayama, Specific genomic sequences of *E. coli* promote replicational initiation by directly reactivating ADP-DnaA. *Genes Dev.* **23**, 1221–1233 (2009).
16. K. Sekimizu, A. Kornberg, Cardiolipin activation of DnaA protein, the initiation protein of replication in *Escherichia coli*. *J. Biol. Chem.* **263**, 7131–7135 (1988).
17. K. Kasho, T. Katayama, DnaA binding locus *datA* promotes DnaA-ATP hydrolysis to enable cell cycle-coordinated replication initiation. *Proc. Natl. Acad. Sci. U.S.A.* **110**, 936–941 (2013).
18. J. I. Kato, T. Katayama, Hda, a novel DnaA-related protein, regulates the replication cycle in *Escherichia coli*. *EMBO J.* **20**, 4253–4262 (2001).
19. T. A. Rozgaja, J. E. Grimwade, M. Iqbal, C. Czerwonka, M. Vora, A. C. Leonard, Two oppositely oriented arrays of low-affinity recognition sites in *oriC* guide progressive binding of DnaA during *Escherichia coli* pre-RC assembly. *Mol. Microbiol.* **82**, 475–488 (2011).
20. J. E. Grimwade, T. A. Rozgaja, R. Gupta, K. Dyson, P. Rao, A. C. Leonard, Origin recognition is the predominant role for DnaA-ATP in initiation of chromosome replication. *Nucleic Acids Res.* **46**, 6140–6151 (2018).
21. S. Ozaki, H. Kawakami, K. Nakamura, N. Fujikawa, W. Kagawa, S. Y. Park, S. Yokoyama, H. Kurumizaka, T. Katayama, A common mechanism for the ATP-DnaA-dependent formation of open complexes at the replication origin. *J. Biol. Chem.* **283**, 8351–8362 (2008).
22. N. S. Hill, R. Kadoya, D. K. Chattoraj, P. A. Levin, Cell size and the initiation of DNA replication in bacteria. *PLOS Genet.* **8**, e1002549 (2012).
23. L. Sompayrac, O. Maaløe, Autorepressor model for control of DNA replication. *Nat. New Biol.* **241**, 133–135 (1973).
24. F. G. Hansen, B. B. Christensen, T. Atlung, The initiator titration model: Computer simulation of chromosome and minichromosome control. *Res. Microbiol.* **142**, 161–167 (1991).
25. L. Olivi, S. Köstlbacher, C. Ludwig, M. Langendoen, N. J. Claassens, T. J. G. Ettema, J. van der Oost, P. R. ten Wolde, J. Hohlbein, R. H. J. Staals, The *Escherichia coli* replication initiator DnaA is titrated on the chromosome. *Nat. Commun.* **16**, 7813 (2025).
26. M. Berger, P. R. ten Wolde, Robust replication initiation from coupled homeostatic mechanisms. *Nat. Commun.* **13**, 6556 (2022).
27. H. Fu, F. Xiao, S. Jun, Bacterial replication initiation as precision control by protein counting. *PRX Life* **1**, 013011 (2023).
28. I. Iuliani, G. Mbemba, M. C. Lagomarsino, B. Sclavi, Direct single-cell observation of a key *Escherichia coli* cell-cycle oscillator. *Sci. Adv.* **10**, eado5398 (2024).
29. T. Katayama, The mutant DnaAcos protein which overinitiates replication of the *Escherichia coli* chromosome is inert to negative regulation for initiation. *J. Biol. Chem.* **269**, 22075–22079 (1994).
30. G. Kellenberger-Gujer, A. J. Podhajska, L. Caro, A cold sensitive *dnaA* mutant of *E. coli* which overinitiates chromosome replication at low temperature. *MGG. Mol. Gen. Genet.* **162**, 9–16 (1978).

Downloaded from https://www.science.org at AMOLF on November 11, 2026

31. R. E. Braun, K. O'Day, A. Wright, Cloning and characterization of *dnaA*(Cs), a mutation which leads to overinitiation of DNA replication in *Escherichia coli* K-12. *J. Bacteriol.* **169**, 3898–3903 (1987).
32. K. M. Carr, J. M. Kaguni, The A184V missense mutation of the *dnaA5* and *dnaA46* alleles confers a defect in ATP binding and thermolability in initiation of *Escherichia coli* DNA replication. *Mol. Microbiol.* **20**, 1307–1318 (1996).
33. T. Katayama, E. Crooke, K. Sekimizu, Characterization of *Escherichia coli* DnaAcos protein in replication systems reconstituted with highly purified proteins. *Mol. Microbiol.* **18**, 813–820 (1995).
34. S. Klumpp, Z. Zhang, T. Hwa, Growth rate-dependent global effects on gene expression in bacteria. *Cell* **139**, 1366–1375 (2009).
35. J. L. Campbell, N. Kleckner, *E. coli oriC* and the *dnaA* gene promoter are sequestered from Dam methyltransferase following the passage of the chromosomal replication fork. *Cell* **62**, 967–979 (1990).
36. T. Waldminghaus, K. Skarstad, The *Escherichia coli* SeqA protein. *Plasmid* **61**, 141–150 (2009).
37. J. Nordman, O. Skovgaard, A. Wright, A novel class of mutations that affect DNA replication in *E. coli*. *Mol. Microbiol.* **64**, 125–138 (2007).
38. K. Fujimitsu, M. Su'etsugu, Y. Yamaguchi, K. Mazda, N. Fu, H. Kawakami, T. Katayama, Modes of overinitiation, *dnaA* gene expression, and inhibition of cell division in a novel cold-sensitive *hda* mutant of *Escherichia coli*. *J. Bacteriol.* **190**, 5368–5381 (2008).
39. G. Charbon, L. Riber, M. Cohen, O. Skovgaard, K. Fujimitsu, T. Katayama, A. Løbner-Olesen, Suppressors of $DnaA^{ATP}$ imposed overinitiation in *Escherichia coli*. *Mol. Microbiol.* **79**, 914–928 (2011).
40. G. Charbon, C. Campion, S. H. J. Chan, L. Bjørn, A. Weimann, L. C. N. da Silva, P. R. Jensen, A. Løbner-Olesen, Re-wiring of energy metabolism promotes viability during hyperreplication stress in E. coli. *PLOS Genet.* **13**, e1006590 (2017).
41. D. Saluja, G. N. Godson, Biochemical characterization of *Escherichia coli* temperature-sensitive *dnaB* mutants *dnaB8*, *dnaB252*, *dnaB70*, *dnaB43*, and *dnaB454*. *J. Bacteriol.* **177**, 1104–1111 (1995).
42. U. Von Freiesleben, K. V. Rasmussen, T. Atlung, F. G. Hansen, Rifampicin-resistant initiation of chromosome replication from *oriC* in *ihf* mutants. *Mol. Microbiol.* **37**, 1087–1093 (2000).
43. Morigen, F. Molina, K. Skarstad, Skarstad, deletion of the *datA* site does not affect once-per-cell-cycle timing but induces rifampin-resistant replication. *J. Bacteriol.* **187**, 3913–3920 (2005).
44. I. Flåtten, S. Fossum-Raunehaug, R. Taipale, S. Martinsen, K. Skarstad, The DnaA protein is not the limiting factor for initiation of replication in *Escherichia coli*. *PLOS Genet.* **11**, e1005276 (2015).
45. L. Olivi, C. Bagchus, V. Pool, E. Bekkering, K. Speckner, H. Offerhaus, W. Y. Wu, M. Depken, K. J. Martens, R. H. Staals, J. Hohlbein, Live-cell imaging reveals the trade-off between target search flexibility and efficiency for Cas9 and Cas12a. *Nucleic Acids Res.* **52**, 5241–5256 (2024).
46. H. Zheng, P.-Y. Ho, M. Jiang, B. Tang, W. Liu, D. Li, X. Yu, N. E. Kleckner, A. Amir, C. Liu, Interrogating the *Escherichia coli* cell cycle by cell dimension perturbations. *Proc. Natl. Acad. Sci. U.S.A.* **113**, 15000–15005 (2016).
47. M. Berger, P. R. ten Wolde, Synchronous replication initiation of multiple origins. *PRX Life* **1**, 013007 (2023).
48. D. Li, H. Zheng, Y. Bai, Z. Zhang, H. Cheng, X. Huang, T. Wei, M. Chang, A. Zaritsky, T. Hwa, C. Liu, Extrusion-modulated DnaA activity oscillations coordinate DNA replication with biomass growth. *ELife* **14**, RP107214 (2025).
49. J. C. Guimaraes, M. Rocha, A. P. Arkin, Transcript level and sequence determinants of protein abundance and noise in *Escherichia coli*. *Nucleic Acids Res.* **42**, 4791–4799 (2014).
50. P. Lu, C. Vogel, R. Wang, X. Yao, E. M. Marcotte, Absolute protein expression profiling estimates the relative contributions of transcriptional and translational regulation. *Nat. Biotechnol.* **25**, 117–124 (2007).
51. J. H. LeBowitz, R. McMacken, The *Escherichia coli* DnaB replication protein is a DNA helicase. *J. Biol. Chem.* **261**, 4738–4748 (1986).
52. O. Skovgaard, M. Bak, A. Løbner-Olesen, N. Tommerup, Genome-wide detection of chromosomal rearrangements, indels, and mutations in circular chromosomes by short read sequencing. *Genome Res.* **21**, 1388–1393 (2011).
53. S. Gon, J. E. Camara, H. K. Klungsøyr, E. Crooke, K. Skarstad, J. Beckwith, A novel regulatory mechanism couples deoxyribonucleotide synthesis and DNA replication in *Escherichia coli*. *EMBO J.* **25**, 1137–1147 (2006).
54. V. M. P. Babu, M. Itsko, J. C. Baxter, R. M. Schaaper, M. D. Sutton, Insufficient levels of the *nrdAB*-encoded ribonucleotide reductase underlie the severe growth defect of the Δ*hda E. coli* strain. *Mol. Microbiol.* **104**, 377–399 (2017).
55. G. Charbon, L. Bjørn, B. Mendoza-Chamizo, J. Frimodt-Møller, A. Løbner-Olesen, Oxidative DNA damage is instrumental in hyperreplication stress-induced inviability of *Escherichia coli*. *Nucleic Acids Res.* **42**, 13228–13241 (2014).
56. Y. Noguchi, T. Katayama, The *Escherichia coli* cryptic prophage protein YfdR binds to DnaA and initiation of chromosomal replication is inhibited by overexpression of the gene cluster *yfdQ-yfdR-yfdS-yfdT*. *Front. Microbiol.* **7**, 239 (2016).
57. H. Shinagawa, H. Iwasaki, Y. Ishino, A. Nakata, SOS-inducible DNA polymerase II of *E. coli* is homologous to replicative DNA polymerase of eukaryotes. *Biochimie* **73**, 433–435 (1991).
58. R. Napolitano, R. Janel-Bintz, J. Wagner, R. P. P. Fuchs, All three SOS-inducible DNA polymerases (Pol II, Pol IV and Pol V) are involved in induced mutagenesis. *EMBO J.* **19**, 6259–6265 (2000).
59. J. J. Truglio, D. L. Croteau, B. Van Houten, C. Kisker, Prokaryotic nucleotide excision repair: The UvrABC system. *Chem. Rev.* **106**, 233–252 (2006).
60. M. Tang, X. Shen, E. G. Frank, M. O'Donnell, R. Woodgate, M. F. Goodman, $UmuD'_2$ C is an error-prone DNA polymerase, *Escherichia coli* pol V. *Proc. Natl. Acad. Sci. U.S.A.* **96**, 8919–8924 (1999).
61. N. B. Reuven, G. Arad, A. Maor-Shoshani, Z. Livneh, The mutagenesis protein UmuC is a DNA polymerase activated by UmuD′, RecA, and SSB and is specialized for translesion replication. *J. Biol. Chem.* **274**, 31763–31766 (1999).
62. J. C. Bell, S. C. Kowalczykowski, RecA: Regulation and mechanism of a molecular search engine. *Trends Biochem. Sci.* **41**, 491–507 (2016).
63. L. B. Augustin, B. A. Jacobson, J. A. Fuchs, *Escherichia coli* Fis and DnaA proteins bind specifically to the *nrd* promoter region and affect expression of an *nrd-lac* fusion. *J. Bacteriol.* **176**, 378–387 (1994).
64. A. M. Stringer, D. M. Fitzgerald, J. T. Wade, Mapping the *Escherichia coli* DnaA-binding landscape reveals a preference for binding pairs of closely spaced DNA sites. *Microbiology* **170**, 001474 (2024).
65. E. Torrents, I. Grinberg, B. Gorovitz-Harris, H. Lundström, I. Borovok, Y. Aharonowitz, B.-M. Sjöberg, G. Cohen, NrdR controls differential expression of the *Escherichia coli* ribonucleotide reductase genes. *J. Bacteriol.* **189**, 5012–5021 (2007).
66. E. Rotman, S. R. Khan, E. Kouzminova, A. Kuzminov, Replication fork inhibition in *seqA* mutants of *Escherichia coli* triggers replication fork breakage. *Mol. Microbiol.* **93**, 50–64 (2014).
67. A. Knöppel, O. Broström, K. Gras, J. Elf, D. Fange, Regulatory elements coordinating initiation of chromosome replication to the *Escherichia coli* cell cycle. *Proc. Natl. Acad. Sci. U.S.A.* **120**, e2213795120 (2023).
68. P. Wang, L. Robert, J. Pelletier, W. L. Dang, F. Taddei, A. Wright, S. Jun, Robust growth of *Escherichia coli*. *Curr. Biol.* **20**, 1099–1103 (2010).
69. J. M. Pennington, S. M. Rosenberg, Spontaneous DNA breakage in single living *Escherichia coli* cells. *Nat. Genet.* **39**, 797–802 (2007).
70. L. Olivi, M. Berger, R. N. P. Creyghton, N. D. Franceschi, C. Dekker, B. M. Mulder, N. J. Claassens, P. R. ten Wolde, J. van der Oost, Towards a synthetic cell cycle. *Nat. Commun.* **12**, 4531 (2021).
71. L. Willis, K. C. Huang, Sizing up the bacterial cell cycle. *Nat. Rev. Microbiol.* **15**, 606–620 (2017).
72. N. J. Gaut, K. P. Adamala, Reconstituting natural cell elements in synthetic cells. *Adv. Biol.* **5**, e2000188 (2021).
73. M. Salas, I. Holguera, M. Redrejo-Rodríguez, M. de Vega, DNA-binding proteins essential for protein-primed bacteriophage Φ29 DNA replication. *Front. Mol. Biosci.* **3**, 37 (2016).
74. C. G. Sokolik, M. Bar-Dolev, R. Milo, K. P. Adamala, M. Levy, Synthetic cells by the numbers. *IScience* **28**, 113849 (2025).
75. C. C. Koster, H. da Costa Oliveira, F. van Beveren, J. Houkes, J. J. E. van Hooff, T. J. G. Ettema, J. van der Oost, N. J. Claassens, De novo design of synthetic microbial genomes. *Nat. Rev. Bioeng.* **4**, 523–540 (2026).
76. L. Blanco, A. Bernad, J. M. Lázaro, G. Martín, C. Garmendia, M. Salas, Highly efficient DNA synthesis by the phage ϕ 29 DNA polymerase: Symmetrical mode of DNA replication. *J. Biol. Chem.* **264**, 8935–8940 (1989).
77. Z. Abil, C. Danelon, Roadmap to building a cell: An evolutionary approach. *Front. Bioeng. Biotechnol.* **8**, 927 (2020).
78. G. M. Cooper, "The eukaryotic cell cycle," in *The Cell: A Molecular Approach. 2nd Edition* (Sinauer Associates Inc., 2000); https://ncbi.nlm.nih.gov/books/NBK9876/.
79. K. A. Datsenko, B. L. Wanner, One-step inactivation of chromosomal genes in *Escherichia coli* K-12 using PCR products. *Proc. Natl. Acad. Sci. U.S.A.* **97**, 6640–6645 (2000).
80. H. Albert, E. C. Dale, E. Lee, D. W. Ow, Site-specific integration of DNA into wild-type and mutant lox sites placed in the plant genome. *Plant J.* **7**, 649–659 (1995).
81. S. C. A. Creutzburg, Structure-function relations of RNA molecules involved in gene expression and host defence. (2020); https://doi.org/10.18174/532325.
82. S. Wenk, O. Yishai, S. N. Lindner, A. Bar-Even, An engineering approach for rewiring microbial metabolism. *Methods Enzymol.* **608**, 329–367 (2018).
83. J. Doellinger, A. Schneider, M. Hoeller, P. Lasch, Sample preparation by easy extraction and digestion (SPEED)—A universal, rapid, and detergent-free protocol for proteomics based on acid extraction. *Mol. Cell. Proteomics* **19**, 209–222 (2020).
84. M. Abele, E. Doll, F. P. Bayer, C. Meng, N. Lomp, K. Neuhaus, S. Scherer, B. Kuster, C. Ludwig, Unified workflow for the rapid and in-depth characterization of bacterial proteomes. *Mol. Cell. Proteomics* **22**, 100612 (2023).
85. C. Wu, M. Mori, M. Abele, A. Banaei-Esfahani, Z. Zhang, H. Okano, R. Aebersold, C. Ludwig, T. Hwa, Enzyme expression kinetics by *Escherichia coli* during transition from rich to minimal media depends on proteome reserves. *Nat. Microbiol.* **8**, 347–359 (2023).

Downloaded from https://www.science.org at AMOLF on November 11, 2026

86. V. Demichev, C. B. Messner, S. I. Vernardis, K. S. Lilley, M. Ralser, DIA-NN: Neural networks and interference correction enable deep proteome coverage in high throughput. *Nat. Methods* **17**, 41–44 (2020).
87. M.-A. Gerault, L. Camoin, S. Granjeaud, DIAgui: A Shiny application to process the output from DIA-NN. *Bioinform. Adv.* **4**, vbae001 (2024).
88. B. Schwanhäusser, D. Busse, N. Li, G. Dittmar, J. Schuchhardt, J. Wolf, W. Chen, M. Selbach, Global quantification of mammalian gene expression control. *Nature* **473**, 337–342 (2011).
89. J. Cox, M. Y. Hein, C. A. Luber, I. Paron, N. Nagaraj, M. Mann, Accurate proteome-wide label-free quantification by delayed normalization and maximal peptide ratio extraction, termed MaxLFQ. *Mol. Cell. Proteomics* **13**, 2513–2526 (2014).
90. C. Meng, Fast analyzing, exploring and sharing quantitative omics data using omicsViewer. bioRxiv 483845 [Preprint] (2022). https://doi.org/10.1101/2022.03.10.483845.
91. K. J. Cutler, C. Stringer, T. W. Lo, L. Rappez, N. Stroustrup, S. Brook Peterson, P. A. Wiggins, J. D. Mougous, Omnipose: A high-precision morphology-independent solution for bacterial cell segmentation. *Nat. Methods* **19**, 1438–1448 (2022).
92. H. Bremer, G. Churchward, An examination of the Cooper-Helmstetter theory of DNA replication in bacteria and its underlying assumptions. *J. Theor. Biol.* **69**, 645–654 (1977).
93. D. J. Ferullo, D. L. Cooper, H. R. Moore, S. T. Lovett, Cell cycle synchronization of *Escherichia coli* using the stringent response, with fluorescence labeling assays for DNA content and replication. *Methods* **48**, 8–13 (2009).
94. H. Li, Minimap2: Pairwise alignment for nucleotide sequences. *Bioinformatics* **34**, 3094–3100 (2018).
95. P. Danecek, J. K. Bonfield, J. Liddle, J. Marshall, V. Ohan, M. O. Pollard, A. Whitwham, T. Keane, S. A. McCarthy, R. M. Davies, H. Li, Twelve years of SAMtools and BCFtools. *Gigascience* **10**, giab008 (2021).
96. J. Brochu, É. Vlachos-Breton, D. Irsenco, M. Drolet, Characterization of a pathway of genomic instability induced by R-loops and its regulation by topoisomerases in *E. coli*. *PLOS Genet.* **19**, e1010754 (2023).

Acknowledgments: We would like to thank F. Hackbarth and T. Midari for technical assistance and maintenance of mass spectrometers. We would like to thank H. Heilig for technical assistance on performing all digital PCR experiments. We would like to thank O. Broström and D. Fange for constructive discussions and a critical reading of the manuscript. **Funding:** L.O., N.J.C., J.v.d.O., and P.R.t.W. acknowledge financial support from The Netherlands Organization of Scientific Research (NWO/OCW) Gravitation program Building a Synthetic Cell (BaSyC) (024.003.019) and Summit program "Evolving life from non-life" (EVOLF) (SUMMIT.1.004). The Exploris 480 mass spectrometer was funded in part by the German Research Foundation (INST 95/1435-1 FUGG).
Author contributions: Conceptualization: M.B., P.R.t.W., and L.O. Methodology: B.A.-P., C.L., D.F., P.R.t.W., and L.O. Software: D.F., J.H., and L.O. Validation: B.A.-P., C.L., A.A.S., and L.O. Investigation: B.A.-P., C.L., A.A.S., and L.O. Formal analysis: C.L. and L.O. Visualization: B.A.-P. and L.O. Data curation: B.A.-P. and L.O. Supervision: J.H., R.H.J.S., P.R.t.W., N.J.C., and L.O. Writing—original draft: B.A.-P., R.H.J.S., and L.O. Writing—review and editing: B.A.-P., C.L., D.F., M.B., J.H., R.H.J.S., P.R.t.W., J.v.d.O., N.J.C., and L.O. Resources: C.L., J.H., J.v.d.O., and L.O. Funding acquisition: P.R.t.W., J.v.d.O., and N.J.C. Project administration: L.O. **Competing interests:** The authors declare that they have no competing interests. **Data, code, and materials availability:** All data and code needed to evaluate and reproduce the results in the paper are present in the paper, the Supplementary Materials, and/or the repositories listed here. The mass spectrometric raw files as well as the DIA-NN output files have been deposited in the ProteomeXchange Consortium via the PRIDE partner repository and can be accessed using the identifier PXD075568 (https://proteomecentral.proteomexchange.org/cgi/GetDataset?ID=PXD075568). Raw reads of sequencing used for marker frequency analysis, as well as the MATLAB script used to analyze them and generate figures, have been deposited in Zenodo (https://doi.org/10.5281/zenodo.21934166). Newly generated materials in the form of mutant bacterial strains and plasmids are available from L.O. (lorenzo.olivi@icm.uu.se) on reasonable request.

Submitted 18 May 2026
Accepted 10 September 2026
Published 16 October 2026
10.1126/sciadv.aei9788

Downloaded from https://www.science.org at AMOLF on November 11, 2026

Science Advances

Establishment of titration-based control of DNA replication in *Escherichia coli*

Belén Adiego-Pérez, Christina Ludwig, Demian Fluit, Mareike Berger, Alejandra Alonso Santirso, Johannes Hohlbein, Raymond H. J. Staals, Pieter Rein ten Wolde, John van der Oost, Nico J. Claassens, and Lorenzo Olivi

Sci. Adv. **12** (42), eaei9788. DOI: 10.1126/sciadv.aei9788

View the article online
https://www.science.org/doi/10.1126/sciadv.aei9788
Permissions
https://www.science.org/help/reprints-and-permissions

Downloaded from https://www.science.org at AMOLF on November 11, 2026

Use of this article is subject to the Terms of service

Science Advances (ISSN 2375-2548) is published by the American Association for the Advancement of Science. 1200 New York Avenue NW, Washington, DC 20005. The title *Science Advances* is a registered trademark of AAAS.

Copyright © 2026 The Authors, some rights reserved; exclusive licensee American Association for the Advancement of Science. No claim to original U.S. Government Works. Distributed under a Creative Commons Attribution License 4.0 (CC BY).